Cell cycle–dependent spatial segregation of telomerase from sites of DNA damage

Faissal Ouenzar,* Maxime Lalonde,* Hadrien Laprade, Geneviève Morin, Franck Gallardo, Samuel Tremblay-Belzile, and Pascal Chartrand

Department of Biochemistry and Molecular Medicine, Université de Montréal, Montréal, Quebec, Canada

Telomerase can generate a novel telomere at DNA double-strand breaks (DSBs), an event called de novo telomere addition. How this activity is suppressed remains unclear. Combining single-molecule imaging and deep sequencing, we show that the budding yeast telomerase RNA (*TLC1* RNA) is spatially segregated to the nucleolus and excluded from sites of DNA repair in a cell cycle–dependent manner. Although *TLC1* RNA accumulates in the nucleoplasm in G1/S, Pif1 activity promotes *TLC1* RNA localization in the nucleolus in G2/M. In the presence of DSBs, *TLC1* RNA remains nucleolar in most G2/M cells but accumulates in the nucleoplasm and colocalizes with DSBs in *rad52Δ* cells, leading to de novo telomere additions. Nucleoplasmic accumulation of *TLC1* RNA depends on Cdc13 localization at DSBs and on the SUMO ligase Siz1, which is required for de novo telomere addition in *rad52Δ* cells. This study reveals novel roles for Pif1, Rad52, and Siz1-dependent sumoylation in the spatial exclusion of telomerase from sites of DNA repair.

Introduction

DNA double-strand breaks (DSBs) are one of the most cytotoxic forms of DNA damage, and their repair is critical for maintenance of genome integrity and cell survival. Classically, two pathways of DSB repair have been defined: nonhomologous end joining (NHEJ) and homologous recombination (HR). NHEJ, which occurs preferentially in G1, directly rejoins the DNA ends and often results in loss of genetic information at the break site (Moore and Haber, 1996; Takata et al., 1998). HR, which occurs during S and G2 phase, requires an homologous template for repair and generally preserves genetic information at the break site (Moore and Haber, 1996; Pâques and Haber, 1999). The choice of DSB repair by the HR or NHEJ pathway is dictated in part by the presence or absence of 5′-to-3′ resection, which generates 3′ single-stranded DNA (ssDNA) tails at the DSB ends and commits DSB repair to HR.

In addition to HR and NHEJ, DSBs can be repaired by the action of telomerase at the break site, a phenomenon referred to as telomere healing or de novo telomere addition, which often leads to gross chromosomal rearrangements (GCRs; Kramer and Haber, 1993; Pennaneach et al., 2006). Telomere healing has been particularly well studied in the budding yeast *Saccharomyces cerevisiae*. In yeast, telomerase is composed of an RNA moiety called *TLC1*, which contains the template sequence and acts as scaffold on which the catalytic reverse transcription Est2 and associated proteins (Est1, Est3, and yKu70/80) bind (Singer and Gottschling, 1994; Counter et al., 1997; Lingner et al., 1997). Recruitment of telomerase to telomeres during S phase depends on the interaction between Est1 and the telomeric DNA single-strand binding protein Cdc13 (Pennock et al., 2001; Bianchi et al., 2004; Bianchi and Shore, 2008).

Telomere healing events in yeast are suppressed by numerous mechanisms. One includes the 5′–3′ DNA helicase Pif1 that acts as a potent inhibitor of telomere addition at telomeres and DSBs (Schulz and Zakian, 1994; Zhou et al., 2000). Pif1-deficient cells have overelongated telomeres and a rate of telomere healing that is dramatically increased compared with WT cells (Myung et al., 2001). Pif1 is phosphorylated upon DNA damage in a Mec1-dependent manner, and a phosphorylation-defective mutant of Pif1 (*pif1-4A*) displays an increased propensity to add telomeric repeats on an HO endonuclease–induced DSB (Makovets and Blackburn, 2009). In addition to Pif1, the Mec1 kinase phosphorylates Cdc13 on its S306 residue, a phosphorylation event suggested to suppress Cdc13 recruitment to DSB ends that have little or no telomere-like sequences (Zhang and Durocher, 2010). However, recent evidence shows that these mechanisms are not sufficient to repress all Cdc13 and telomerase recruitment events at DSBs because Cdc13 and telomerase subunits can be detected at a DSB by chromatin immunoprecipitation, even if no telomere is

*F. Ouenzar and M. Lalonde contributed equally to this paper.

Correspondence to Pascal Chartrand: p.chartrand@umontreal.ca

F. Ouenzar's present address is Dept. of Oncology, University of Alberta, Edmonton, Canada.

F. Gallardo's present address is NeoVirTech, Toulouse, France.

Abbreviations used: DIC, differential interference contrast; DSB, double-strand break; GCR, gross chromosomal rearrangement; HR, homologous recombination; IF, immunofluorescence; NHEJ, nonhomologous end joining; rDNA, ribosomal DNA; ssDNA, single-stranded DNA; YEPD, yeast extract peptone-dextrose.

The Rockefeller University Press
J. Cell Biol. Vol. 216 No. 8 2355–2371
https://doi.org/10.1083/jcb.201610071

added to the break (Oza et al., 2009; Chung et al., 2010; McGee et al., 2010; Ribaud et al., 2012).

These results suggest a competition between de novo telomere addition and other repair pathways. Indeed, decreased resection by simultaneous deletion of *SGS1* and *EXO1* partially affects HR and increases de novo telomere formation via the recruitment of Cdc13 to the break site (Chung et al., 2010; Lydeard et al., 2010), suggesting that Cdc13 binding to DSB might be a limiting factor for telomere addition. In agreement with this, artificial binding of Cdc13 or Est1 subunit to an HO-induced DSB increases the repair of DSB by telomerase (Bianchi et al., 2004). Another factor involved in HR that affects de novo telomere addition is Rad52, although its role in this process is controversial. Indeed, deletion of *RAD52* does not increase spontaneous telomere addition at HO-induced or spontaneous DSB in yeast (Kramer and Haber, 1993; Mangahas et al., 2001; Myung et al., 2001). However, deletion of *RAD52* increases the frequency of telomere addition in subtelomeric regions (Ricchetti et al., 2003). Furthermore, the deletion of *RAD52* acts synergistically with the *pif1-m2* mutation, an allele that reduces the nuclear activity of Pif1, to increase de novo telomere addition (Myung et al., 2001), suggesting a specific but still unknown role for Rad52 in the suppression of telomere healing.

Previous studies on telomere healing were performed using methods that measure telomerase recruitment or de novo telomere elongation at a single unrepaired endonuclease-induced DSB (Ribeyre and Shore, 2013). Although these approaches revealed extensive mechanistic details on this process, they also showed that sequences surrounding the DNA break and location of the break in the chromosome affect the efficacy by which telomerase recruitment and telomere healing can occur (Ribeyre and Shore, 2013). However, novel approaches are needed to study the behavior, dynamics, and regulation of telomerase molecules in the presence of random breaks in the genome.

In this study, we address this question by visualizing the spatial distribution of telomerase molecules in the presence of random DSBs using single-molecule fluorescent in situ hybridization on endogenous *TLC1* RNA. With this approach, we found that *TLC1* RNA is engaged in an intranuclear trafficking during the cell cycle, as it accumulates in the nucleoplasm in G1/S, whereas it localizes preferentially in the nucleolus in G2/M. This trafficking depends on the helicase Pif1, suggesting a role for this process in the regulation of de novo telomere addition. Indeed, treatment with the radiomimetic drug bleomycin increases the presence of *TLC1* RNA molecules in the nucleoplasm in G2/M cells. We show that Rad52 suppresses the nucleoplasmic localization of *TLC1* RNA in G2/M by inhibiting Cdc13 accumulation at DSBs. Furthermore, we found that the SUMO E3 ligase Siz1 regulates the nucleoplasmic accumulation of *TLC1* RNA and de novo telomere addition without affecting Cdc13 accumulation at DSBs. Altogether, our data show that Pif1, Rad52, and Siz1 act together to control the accumulation of *TLC1* RNA and Cdc13 at DSBs and spatially exclude telomerase into the nucleolus, away from sites of DNA repair.

Results

TLC1 RNA nuclear distribution varies during the cell cycle

Previous studies used FISH to show that *TLC1* RNA accumulates in the nucleoplasm in G1 and S phase, which is related to its function in telomere elongation (Teixeira et al., 2002; Gallardo et al., 2008). Because the telomerase RNA is the limiting component of the telomerase holoenzyme in yeast (Mozdy and Cech, 2006), its dynamics should reflect the dynamics of the active telomerase complex in vivo better than other telomerase components. However, a systematic analysis of the distribution of *TLC1* RNA in each phase of the cell cycle has not yet been conducted. To do so, quantification of telomerase RNA in the nucleus of yeast cells at different phases of the cell cycle was performed using FISH on the endogenous *TLC1* RNA. Budding index was used to determine the cell cycle phase of each cell. Beside *TLC1* RNA, the yeast nucleolus was detected using a probe against the *ITS1* ribosomal RNA spacer precursor, and the nucleoplasm was labeled using DAPI. We detected between 3 and 10 nuclear *TLC1* RNA foci per cell, with each focus corresponding to a single *TLC1* RNA molecule, as recently reported (Bajon et al., 2015). Although cells in G1 and S phase displayed a nucleoplasmic accumulation of *TLC1* RNA foci, as previously shown (Gallardo et al., 2008), a predominantly nucleolar accumulation of *TLC1* RNA foci was observed in G2/M cells, as shown by colocalization with the *ITS1* ribosomal RNA precursor (Fig. 1, A and B). Accumulation of *TLC1* RNA in the nucleolus in G2/M was further validated by cell synchronization with nocodazole (see Fig. 2 C).

To identify factors required for this intranuclear trafficking of *TLC1* RNA, we focused on factors known to regulate telomere length. One of these factors is the Pif1 5′–3′ helicase, which removes telomerase from telomeres in late S/G2 and acts as a negative regulator of telomerase activity (Schulz and Zakian, 1994; Zhou et al., 2000). Quantification of *TLC1* RNA localization during the cell cycle in a *pif1Δ* strain shows that deletion of *PIF1* inhibits the nucleolar accumulation of *TLC1* RNA in G2/M, as *TLC1* RNA accumulated in the nucleoplasm in all the phases of the cell cycle (Figs. 1 C and S1 A). This result was validated using the *pif1-m2* mutant, an allele with reduced nuclear activity of Pif1 (Schulz and Zakian, 1994). This mutant displays a phenotype midway between WT and *pif1Δ* strains, with *TLC1* RNA present in both nucleoplasm and nucleolus in G2/M (Fig. 1 D and S1B). Altogether, these results suggest that Pif1 promotes the trafficking of *TLC1* RNA from the nucleoplasm to the nucleolus in G2/M.

Regulation of *TLC1* RNA nuclear trafficking by Rad52 after DNA damage

Given that *TLC1* RNA molecules accumulate preferentially in the nucleolus during G2/M, we hypothesized that the nucleolar localization of *TLC1* RNA could reduce the capacity of telomerase to interfere with HR to repair DSBs in G2/M (Diede and Gottschling, 1999). Indeed, in the yeast *S. cerevisiae*, HR is mostly excluded from the nucleolus, and DSBs in ribosomal DNA (rDNA) are repaired by HR in the nucleoplasm, suggesting that HR is exclusively nucleoplasmic (Lisby et al., 2003; Torres-Rosell et al., 2007). Furthermore, Pif1, which promotes the trafficking of *TLC1* RNA to the nucleolus, inhibits de novo telomere addition by telomerase at DSBs (Schulz and Zakian, 1994; Phillips et al., 2015). To test this hypothesis, the distribution of *TLC1* RNA molecules was determined by FISH after induction of DNA damage using bleomycin, a radiomimetic agent that preferentially generates DSBs (Chen and Stubbe, 2005). Yeast cells were exposed to 5 µg/ml bleomycin for 180 min, conditions that cause 90% of the cells to have at least one DSB per cell (Fig. S2 A). After treatment with bleomycin, FISH was

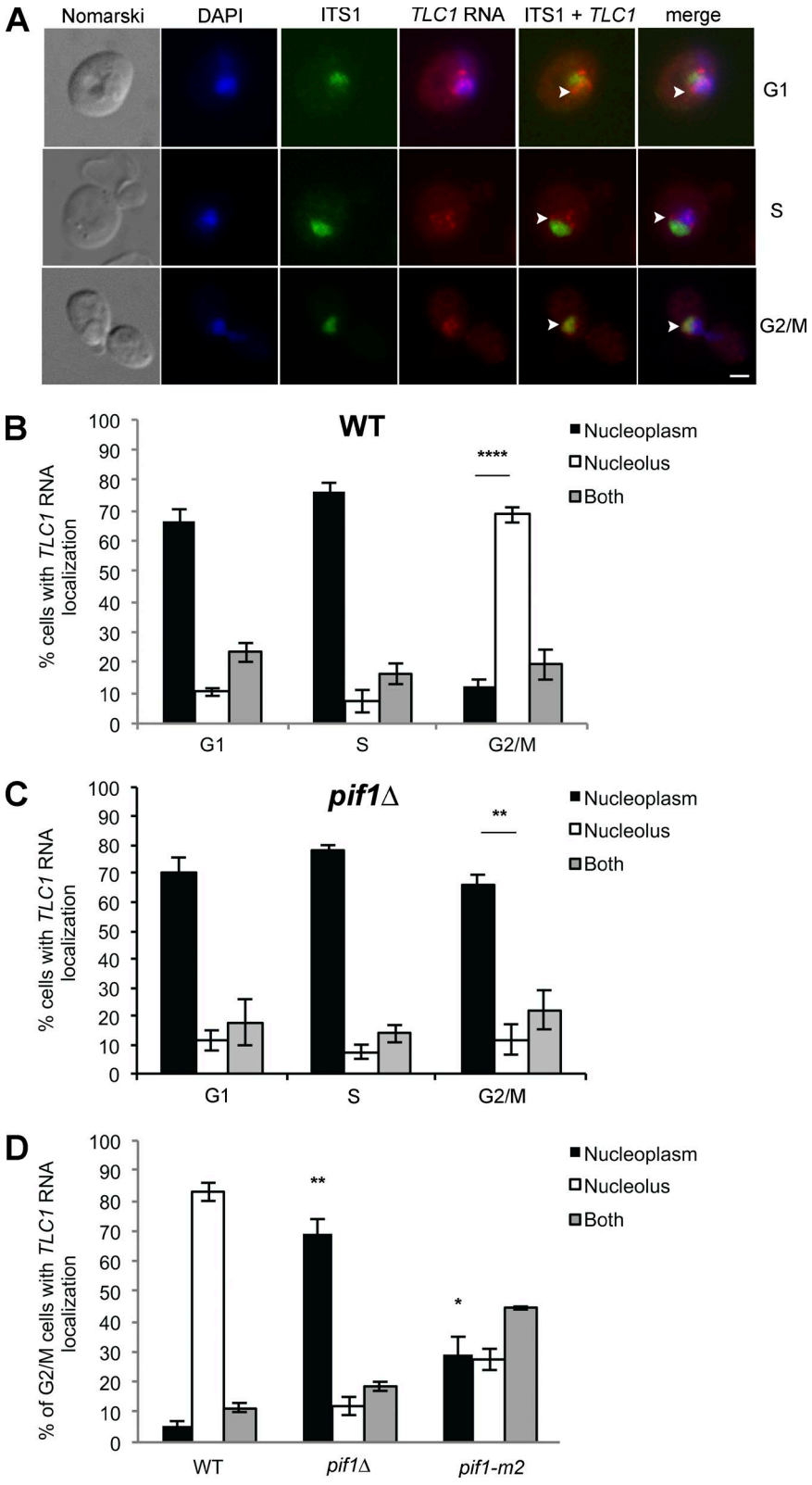

Figure 1. **Intranuclear trafficking of *TLC1* RNA during the cell cycle depends on Pif1.** (A) Monitoring *TLC1* RNA localization during the cell cycle by FISH. The nucleolus was stained with a probe against the *ITS1* spacer of the rRNA precursor (labeled with Cy5). Arrowheads mark the position of the *TLC1* RNA in selected cells. DAPI was used to stain DNA. Bar, 1 µm. (B) Quantification of *TLC1* RNA localization during the cell cycle; n = 900 cells. (C) Quantification of *TLC1* RNA localization during the cell cycle in *pif1Δ* cells; n = 900 cells. (D) Quantification of *TLC1* RNA localization in G2/M in WT, *pif1Δ*, and *pif1-m2* cells; n = 200–900 cells. Error bars represent ±SD. *, P < 0.05; **, P < 0.01; ****, P < 0.001 (two-tailed *t* test).

performed to detect both *TLC1* and *ITS1* RNA. *TLC1* RNA foci remained predominantly nucleolar in both bleomycin treated and untreated G2/M cells (Fig. 2 A). However, quantification of the phenotypes revealed a small but significant accumulation of G2/M cells with *TLC1* RNA in the nucleoplasm in bleomycin-treated cells (Fig. 2 B), suggesting that DNA damage affect the nucleolar distribution of this RNA. To confirm the link between *TLC1* RNA accumulation in the nucleolus and repair of DSB in the nucleoplasm, HR was inhibited by deletion of *RAD52*. Surprisingly, the percentage of G2/M cells with nucleolar *TLC1* RNA foci decreased from 70% in WT cells to 30% in *rad52Δ* cells treated with bleomycin, and most cells accumulated *TLC1*

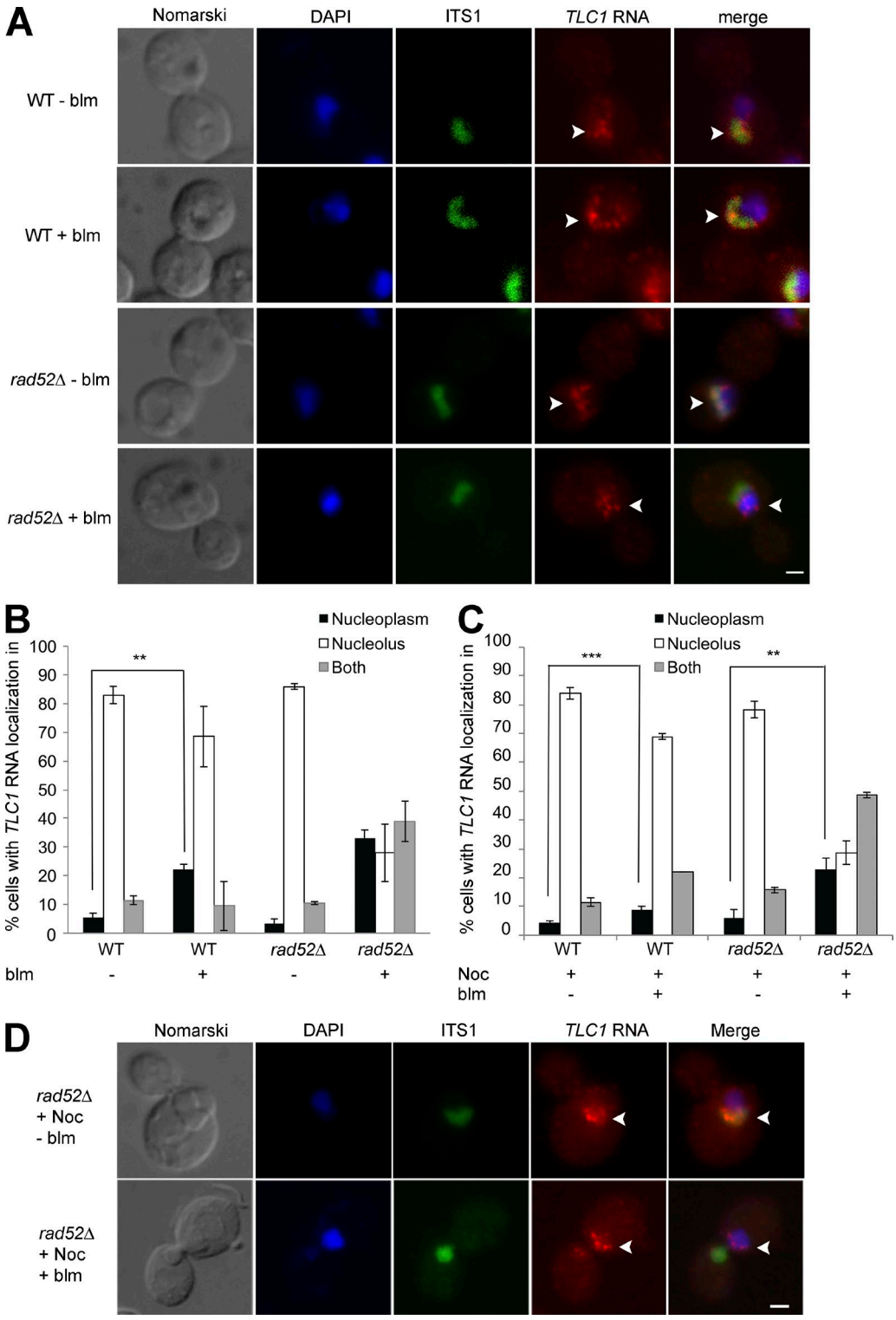

Figure 2. ***TLC1*RNA accumulates in the nucleoplasm in G2/M in *rad52Δ* cells after DNA damage.** (A) FISH on *TLC1* RNA in WT or *rad52Δ* cells treated or not with bleomycin (blm). Arrowheads indicate position of *TLC1* RNA foci in the nucleus. Bar, 1 µm. (B) Quantification of *TLC1* RNA distribution in the nucleus in WT or *rad52Δ* cells after treatment with bleomycin (blm); *n* = 200 cells. (C) *TLC1* RNA can relocalize to the nucleoplasm from the nucleolus in *rad52Δ* cells treated with bleomycin. Quantification of *TLC1* RNA distribution in the nucleus in WT or *rad52Δ* cells synchronized with nocodazole (Noc), followed by treatment with bleomycin (blm); *n* = 200–300 cells. (D) FISH on *TLC1* RNA in *rad52Δ* cells synchronized with nocodazole (Noc) and treated or not with bleomycin (blm). Arrowheads indicate position of *TLC1* RNA foci in cells. Bars, 1 µm. Error bars represent ±SD. **, P < 0.01; ***, P < 0.005 (two-tailed *t* test).

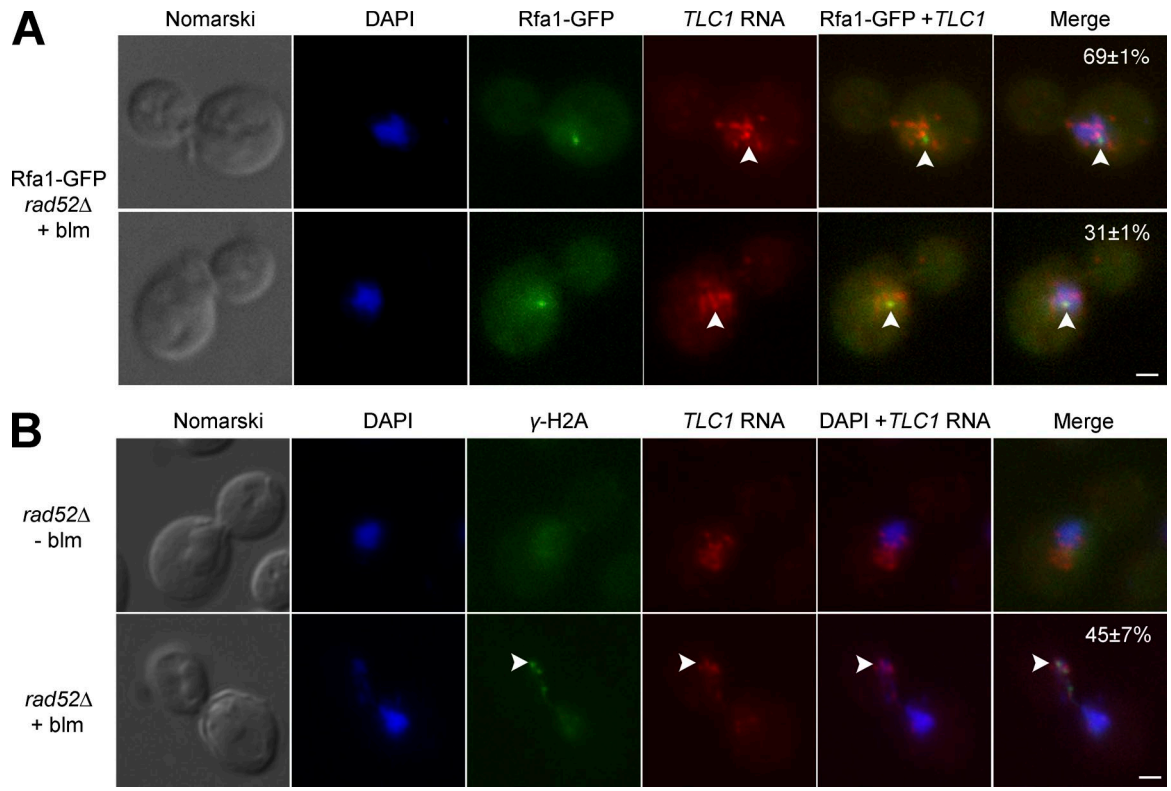

Figure 3. ***TLC1*RNA partially colocalizes with DSB sites in *rad52Δ* cells.** (A) FISH against *TLC1* RNA in *rad52Δ* cells expressing Rfa1-GFP and treated with bleomycin (blm). Numbers in percentages represent the percentage of cells with the following phenotypes: no colocalization between a *TLC1* RNA focus and Rfa1-GFP focus (top) or colocalization between a *TLC1* RNA focus and Rfa1-GFP foci (bottom). Bar, 1 µm; *n* = 200 cells. (B) Dual FISH against *TLC1* RNA and immunofluorescence on γ-H2A protein in *rad52Δ* cells after exposure or not to bleomycin (blm). Colocalization (indicated by arrowheads) was detected in 45 ± 7% of the cells. Bar, 1 µm; *n* = 200 cells.

RNA foci predominantly in the nucleoplasm or in both compartments (Fig. 2, A and B).

To determine if the nucleoplasmic accumulation of *TLC1* RNA in the presence of DSBs is caused by its retention in the nucleoplasm or by its relocalization from the nucleolus to nucleoplasm, yeast cells were synchronized in G2 with nocodazole (Fig. S2 B), followed by treatment with bleomycin. Although nocodazole-treated cells displayed *TLC1* RNA foci in the nucleolus, treatment with bleomycin still resulted in the redistribution of *TLC1* RNA foci toward the nucleoplasm in *rad52Δ* cells, suggesting a dynamic trafficking of this RNA between these two compartments (Fig. 2, C and D). Altogether, these results suggest that in cells containing DSBs, *TLC1* RNA can relocalize from the nucleolus to the nucleoplasm and that its nucleolar retention depends on *RAD52*.

TLC1 RNA colocalizes with DSB sites in the nucleoplasm

To understand the significance of the nucleoplasmic accumulation of *TLC1* RNA in DNA damaged cells devoid of Rad52, the colocalization between *TLC1* RNA and a cytological marker of DSBs was measured. Rfa1, the largest subunit of the heterotrimeric complex RPA, was used as a marker, because it is recruited to DSBs and binds ssDNA generated by resection (Alani et al., 1992; Krogh and Symington, 2004). For this reason, Rfa1 is frequently used as a specific cytological marker for DNA end processing in vivo (Gasior et al., 1998; Raderschall et al., 1999; Barlow et al., 2008). Rfa1 was fused to GFP and, similarly to ionizing radiation–induced DSBs, a single Rfa1-GFP focus was observed in cells treated with bleomycin, in both WT and *rad52Δ* cells (Fig. 3 A). To validate this assay, colocalization between *TLC1* RNA and Rfa1-GFP foci in G2/M was measured in *pif1-m2* cells treated with bleomycin. Because Pif1 plays a key role in removing telomerase from DSBs and inhibits de novo telomere addition (Myung et al., 2001), we expect an increased colocalization between *TLC1* RNA and Rfa1-GFP foci in *pif1-m2* compared with WT cells. Indeed, we observed a colocalization between a Rfa1-GFP focus and a *TLC1* RNA focus in 29% of *pif1-m2* cells treated with bleomycin, whereas such colocalization was observed in 16% of WT cells (Fig. S3 A). FISH was performed on Rfa1-GFP *rad52Δ* cells to detect endogenous *TLC1* RNA after bleomycin treatment. In 31% of the cells, one of the *TLC1* RNA foci colocalized with an Rfa1-GFP focus (Fig. 3 A and Fig. S3 B). This percentage is higher than in WT cells (Fig. S3 A) or compared to the colocalization of *TLC1* RNA foci with a random nuclear focus (corresponding to the *MDN1* transcription site), which colocalize only in 9% of the cells (Fig. S3 C).

It is possible that *TLC1* RNA nucleoplasmic foci that are not colocalized with a Rfa1-GFP focus could be associated with other DNA damage sites (Fig. S3 D). To test this possibility, another cytological marker of DSB, γ-H2A, was combined with FISH on *TLC1* RNA. In contrast to Rfa1-GFP, γ-H2A form several foci in mammalian and yeast cells after DNA damage (Rogakou et al., 1999; Mazumder et al., 2013). In yeast, γ-H2A accumulation is a direct readout of Mec1 activity at a DSB (Ira et al., 2004). Simultaneous FISH against *TLC1* RNA and immunofluorescence (IF) with an antibody specific to γ-H2A

was performed in cells treated or not with bleomycin. In these conditions, yeast cells exposed to 5 µg/ml bleomycin during 180 min contained between two and four γ-H2A foci per cell, whereas untreated cells did not contain any foci (Fig. 3 B). As observed with Rfa1-GFP, most *TLC1* RNA foci were in the nucleoplasm in *rad52Δ* cells treated with bleomycin, but only one *TLC1* RNA focus colocalized with one of the γ-H2A foci in 45% of the cells (Fig. 3 B). Altogether, these results show that during DNA damage and in the absence of Rad52, most *TLC1* RNA molecules are excluded from the nucleolus and accumulate in the nucleoplasm in G2/M, and a fraction of these molecules accumulate at DSBs.

TLC1 RNA nucleoplasmic accumulation after DNA damage depends on Cdc13 and the MRX complex and is regulated by the DNA damage response pathway

The observation that *TLC1* RNA molecules colocalize with only a fraction of the DSBs raises questions concerning the link between *TLC1* RNA trafficking and the DNA damage response. To confirm that *TLC1* RNA accumulation in the nucleoplasm depends on the DNA damage response, factors upstream of Rad52, like the MRX complex (Mre11 and Xrs2), the ATM-like kinase Tel1 and the ATR-like kinase Mec1 were deleted in *rad52Δ* background cells to test their ability to suppress the nucleoplasmic accumulation of *TLC1* RNA (Fig. 4 A). None of these deletions had any effect on the nucleolar distribution of *TLC1* RNA in G2/M cells in the absence of DSBs. After induction of DSBs, deletion of *MRE11* or *XRS2* completely suppressed the nucleoplasmic accumulation of *TLC1* RNA in *rad52Δ* cells (Fig. 4 B). This result is consistent with a function of MRX complex in DSBs processing and de novo telomere addition (Frank et al., 2006). However, deletion of *TEL1* partially suppressed the nucleoplasmic accumulation of *TLC1* RNA in *rad52Δ* cells, as this RNA accumulated in both nucleolus and nucleoplasm (Fig. 4 B). Given the role of Tel1 in DNA resection, it is possible that Tel1 might regulate *TLC1* RNA nucleoplasmic accumulation by positively influencing the function of the MRX complex in the processing of DSBs, as it was shown to do at telomeres (Martina et al., 2012). On the other hand, deletion of *MEC1* has no significant effect on *TLC1* RNA trafficking (Fig. 4 B). Although Mec1 inhibits telomerase activity at DSBs by decreasing Cdc13 binding and by phosphorylation of the telomerase inhibitor Pif1 (Makovets and Blackburn, 2009; Zhang and Durocher, 2010), this activity is not required for *TLC1* RNA trafficking, because this RNA still accumulated in the nucleolus. Altogether, these results are consistent with a model in which DSB processing and resection is required for *TLC1* RNA relocalization from the nucleolus to nucleoplasm in the absence of *RAD52*.

This model predicts that resected DSBs may retain telomerase in the nucleoplasm, and this retention should be mediated by a ssDNA-binding protein. Indeed, the single-strand telomeric binding protein Cdc13 was previously shown to be essential for the recruitment of telomerase at DNA breaks (Bianchi et al., 2004). This was revealed by using the *cdc13-2* mutant, which disrupts the interaction between Cdc13 and the telomerase subunit Est1 (Nugent et al., 1996). We therefore tested the effect of the *cdc13-2* mutation on the distribution of *TLC1* RNA after DNA damage. In a WT *RAD52* background, induction of DSBs in the *cdc13-2* strain reduced the accumulation of *TLC1* RNA in the nucleoplasm compared with a WT strain (Fig. S4 A). This effect is even more striking in a *cdc13-2 rad52Δ* strain, as *TLC1* RNA did not accumulate in the nucleoplasm after exposure to bleomycin, showing that the *cdc13-2* mutation completely suppressed the *rad52Δ* phenotype (Fig. 4, B and C). This result suggests that the Cdc13-Est1 interaction is essential for nucleoplasmic accumulation of *TLC1* RNA after DNA damage.

Cdc13 clusters increase after DNA damage and accumulate at DSB sites

The abovementioned results show that in the absence of Rad52, Cdc13 plays a key role in the nucleoplasmic accumulation of *TLC1* RNA after induction of DSBs. Recent work has shown that Cdc13 can be detected at a DSB by chromatin immunoprecipitation (Oza et al., 2009; Chung et al., 2010; McGee et al., 2010; Ribaud et al., 2012). We therefore examined whether *TLC1* RNA nucleoplasmic accumulation is caused by the accumulation of Cdc13 at DSBs in WT and *rad52Δ* cells. Endogenous Cdc13 was tagged with 13 myc epitopes, and IF was performed to detect the distribution of myc-tagged Cdc13. In WT cells treated with bleomycin, Cdc13-13Myc accumulated as dim subnuclear foci in 20% of G2/M cells (Fig. 5, A and B). Surprisingly, deletion of *RAD52* increased the number of cells with Cdc13 foci to more than 85% (Fig. 5 B). These results were confirmed using a Cdc13-GFP fusion protein in living yeast cells, which revealed the presence of a Cdc13 focus in over 50% of *rad52Δ* cells after bleomycin treatment (Fig. S4 B). The Cdc13 foci formed in *rad52Δ* cells were two- to threefold bigger and brighter than those observed in WT cells (Fig. 5 A and Fig. S4, C and D), likely reflecting an increased number of Cdc13 proteins associated with DSBs. To distinguish the larger Cdc13 foci observed in *rad52Δ* from the dimmer Cdc13 foci, we renamed the larger foci Cdc13 clusters. Notably, these clusters were only formed in *rad52Δ* cells in G2/M after DNA damage, with 65% of the cells containing one cluster and fewer cells containing two clusters (Fig. 5 D), suggesting that Rad52 inhibits Cdc13 accumulation at DSBs. However, we still detected Cdc13 foci in the same percentage of cells in both *rad52Δ* and WT cells (Fig. 5 C).

To determine if Cdc13 accumulates at DSBs after bleomycin addition, the DSB marker Rfa1 was used to investigate the colocalization between Cdc13-GFP and Rfa1-mCherry in G2/M. Cdc13-GFP clusters colocalized with a Rfa1-mCherry focus in 69% of the cells (Fig. 5 E), indicating that Cdc13 accumulates at DSBs. To test if Cdc13 foci/clusters are also formed in the absence of another mediator of HR, such as Rad51, Cdc13 foci/cluster formation was measured in *rad51Δ* cells after bleomycin treatment. Indeed, a previous study had shown that Cdc13 recruitment to an irreparable HO-induced DSB is highly reduced in *rad51Δ* cells (Oza et al., 2009). Strikingly, both Cdc13 foci and clusters disappeared in *rad51Δ* cells (Fig. 5, B and C), whereas *TLC1* RNA accumulated in the nucleolus in those cells (Fig. 5 F), reflecting that Rad51 positively influences Cdc13 accumulation and *TLC1* RNA nucleoplasmic localization at DSBs. To determine the epistatic relationship between *RAD51* and *RAD52* in *TLC1* RNA trafficking, *TLC1* FISH was performed in a double-mutant *rad51Δ rad52Δ* strain. Interestingly, deletion of *RAD51* suppresses the nucleoplasmic accumulation of *TLC1* RNA observed in *rad52Δ* cells, suggesting that *RAD51* is epistatic to *RAD52* in this pathway (Fig. 5 F). Altogether, these results show that nucleoplasmic accumulation of *TLC1* RNA observed in *rad52Δ* cells is linked, in part, to an increased accumulation of Cdc13 at DSBs. In the absence of Rad52, re-

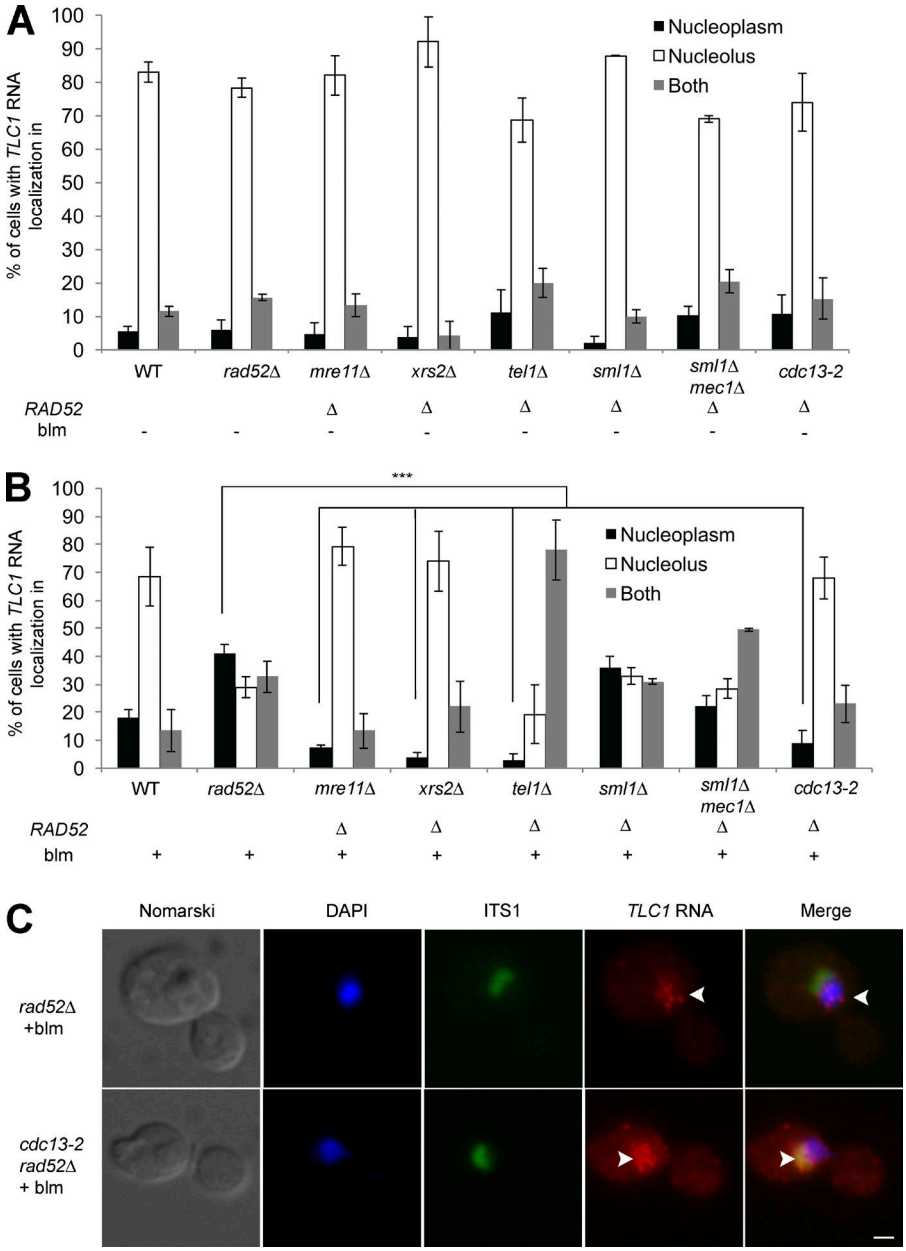

Figure 4. **Genetic requirements for nucleoplasmic accumulation of *TLC1* RNA after DNA damage in *rad52Δ* cells.** (A) *TLC1* RNA does not accumulate in the nucleoplasm in G2/M in the absence of DNA damage in *rad52Δ*, *mre11Δ rad52Δ*; *xrs2Δ rad52Δ*; *tel1Δ rad52Δ*; *sml1Δ rad52Δ*; *sml1Δ mec1Δ rad52Δ* and *cdc13-2 rad52Δ* cells. WT, *rad52Δ*, and *sml1Δrad52Δ* were used as control strains; *n* = 200–300 cells. (B) *TLC1* RNA nucleoplasmic accumulation after induction of DNA damage requires Mre11 and Xrs2 of the MRX complex and Cdc13 and is regulated by Tel1. p-values are included in Table S2. Error bars represent ±SD; *n* = 150–300 cells. (C) FISH on *TLC1* RNA in *cdc13-2 rad52Δ* cells treated or not with bleomycin. Arrowheads indicate the position of *TLC1* RNA foci in cells. Bar, 1 µm. ***, $P < 0.005$ (two-tailed *t* test).

sected DSBs may be more accessible to Cdc13 binding, which may accumulate on the ssDNA and recruit telomerase.

Temporal analysis of Cdc13 foci formation and *TLC1* RNA localization at DNA damage sites

Although the aforementioned data show that Cdc13 and *TLC1* RNA can accumulate at DSBs after induction of DNA damage, it is not clear if their association with DSBs is an early or late event during DNA repair. Indeed, a late recruitment of Cdc13 and *TLC1* RNA would probably suggest an indirect effect caused by the absence of DNA repair at DSBs and the accumulation of longer strands of ssDNA. To answer this question, we measured the kinetics of accumulation of Cdc13 and *TLC1* RNA at DSBs in *rad52Δ* cells. Yeast cells were treated with bleomycin, and culture samples were taken at different time points. Yeast cells were fixed with formaldehyde and processed for IF and/or FISH. Immunofluorescence on Cdc13-myc showed that 50% of the cells already displayed a Cdc13 focus/cluster 30 min after induction of DNA damage (Fig. 6 A). The kinetics of Cdc13 foci/cluster formation was similar to the kinetics of accumulation of γ-H2A foci (Fig. 6 A), suggesting that Cdc13 accumulated rapidly at DSB sites in the absence of Rad52. A refined analysis of Cdc13 accumulation at DSBs was performed by separately quantifying cells with Cdc13 foci or clusters over time. This analysis revealed that the number of cells containing Cdc13 foci reached a peak at 30 min and stayed stable for the remainder of the treatment (Fig. 6 B). Surprisingly, Cdc13 clusters also appeared in over 30% of the cells after 30 min of bleomycin treatment (Fig. 6 B). However, the number of cells containing a Cdc13 cluster still increased over time. These results show that Cdc13's association with DSBs is an early process after DNA damage in the absence of Rad52.

A similar kinetic analysis was performed on *TLC1* RNA using FISH, in which the nucleoplasmic/nucleolar distribution of this RNA was quantified at different time points after induc-

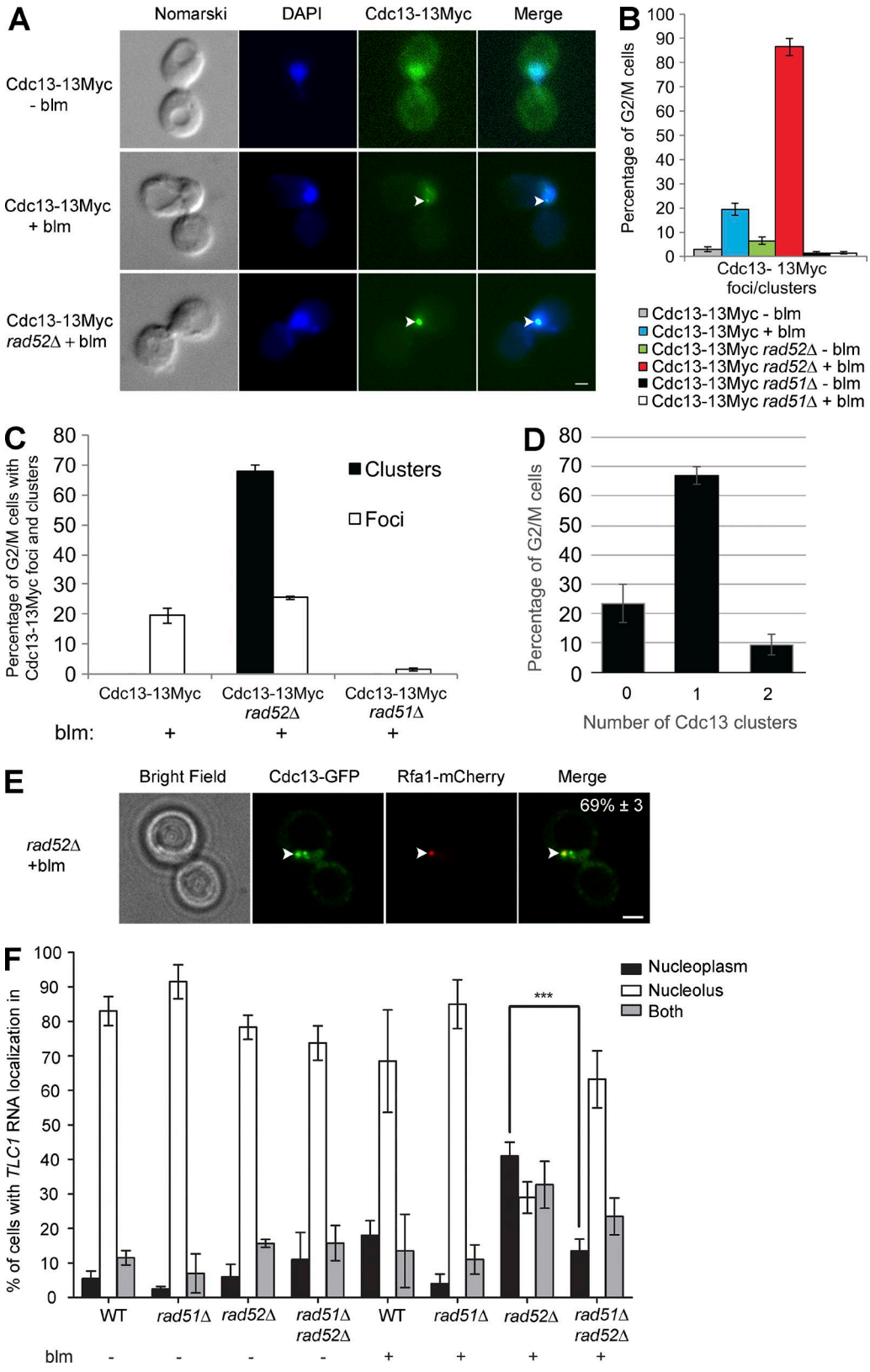

Figure 5. **Cdc13 accumulates at sites of DNA break in *rad52Δ*, but not in *rad51Δ* cells.** (A) Cdc13 foci appear in WT and *rad52Δ* cells after DNA damage. Immunofluorescence (IF) analysis of Cdc13-myc was conducted in WT and *rad52Δ* cells, with or without bleomycin (blm) treatment. Arrowheads mark the position of Cdc13 foci. Bar, 1 µm. (B) Rad52 and Rad51 have opposite effect on Cdc13 foci formation. Quantification of Cdc13 foci/clusters formation in WT, *rad52Δ*, and *rad51Δ* strains, with or without bleomycin (blm) treatment; *n* = 200 cells. (C) Analysis of Cdc13 clusters and foci formation in WT, *rad52Δ*, and *rad51Δ* strains in DNA-damaged cells; *n* = 200 cells. (D) Quantification of the number of Cdc13 cluster per G2/M-damaged cells; *n* = 200

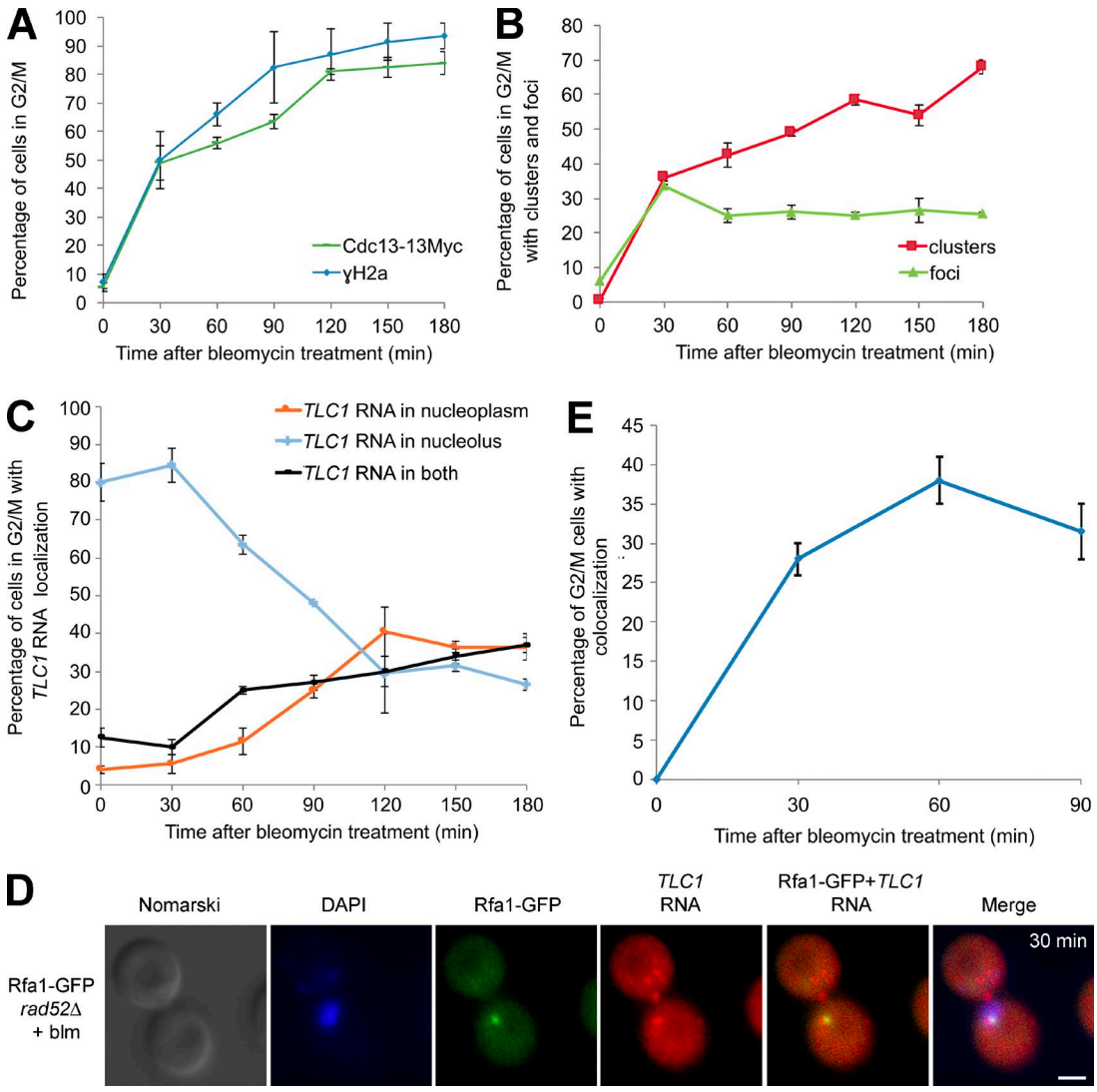

Figure 6. **Kinetics of accumulation of Cdc13 and *TLC1* RNA at sites of DNA damage in*rad52*Δ cells.** (A) Kinetics of γ-H2A and Cdc13 foci formation in G2/M cells after exposure to bleomycin. (B) Time course of Cdc13 foci and cluster formation in G2/M cells after exposure to bleomycin. (C) Kinetics of *TLC1* RNA nucleoplasmic accumulation in G2/M cells after exposure to bleomycin. (D) Colocalization between *TLC1* RNA focus and Rfa1-GFP focus in G2/M cells after 30 min of bleomycin exposure. Bar, 1 µm. (E) Kinetics of colocalization between a *TLC1* RNA focus and a Rfa1-GFP focus in G2/M cells after exposure to bleomycin; *n* = 200 cells per time point. Error bars represent ±SD.

tion of DNA damage. Unlike γ-H2A foci, which accumulated rapidly after DNA damage (Fig. 6 A), the nucleoplasmic accumulation of *TLC1* RNA molecules started later, between 30 and 60 min after bleomycin treatment, and reached a plateau after 120 min (Fig. 6 C). We do not think that the difference in the kinetics of *TLC1* RNA versus γ-H2A is a result of the lower sensitivity of the FISH assay versus IF, because single *TLC1* RNA molecules are detected as single foci with this assay (Bajon et al., 2015). Interestingly, 30 min after induction of DNA damage, *TLC1* RNA remained in the nucleolus even if 50% of the cells contain Cdc13 foci/clusters (Fig. 6, A and C), indicating that the association of Cdc13 with the DNA break sites is not the limiting step for the nucleoplasmic accumulation of *TLC1* RNA.

These results show that nucleoplasmic accumulation of *TLC1* RNA proceeds more slowly than the formation of Cdc13 foci/clusters. However, it is possible that a small number of *TLC1* RNA molecules may associate rapidly with a DSB, whereas the majority of *TLC1* RNA molecules still remain in the nucleolus. To test this possibility, colocalization of *TLC1* RNA with Rfa1-GFP was measured in *rad52Δ* cells during a time-course treatment with bleomycin. Surprisingly, early colocalization of a single *TLC1*

cells. (E) Colocalization of Cdc13-GFP cluster and Rfa1-mCherry focus in *rad52Δ* cell exposed to bleomycin. Arrowheads mark a colocalization event. Percentage of G2/M cells showing this phenotype is indicated in the last panel; *n* = 200 cells. (F) Quantification of *TLC1* RNA distribution in the nucleus in WT, *rad52Δ*, *rad51Δ*, or *rad51Δ rad52Δ* cells after treatment with bleomycin; *n* = 200–344 cells. Error bars represent ±SD. ***, P < 0.005 (two-tailed *t* test).

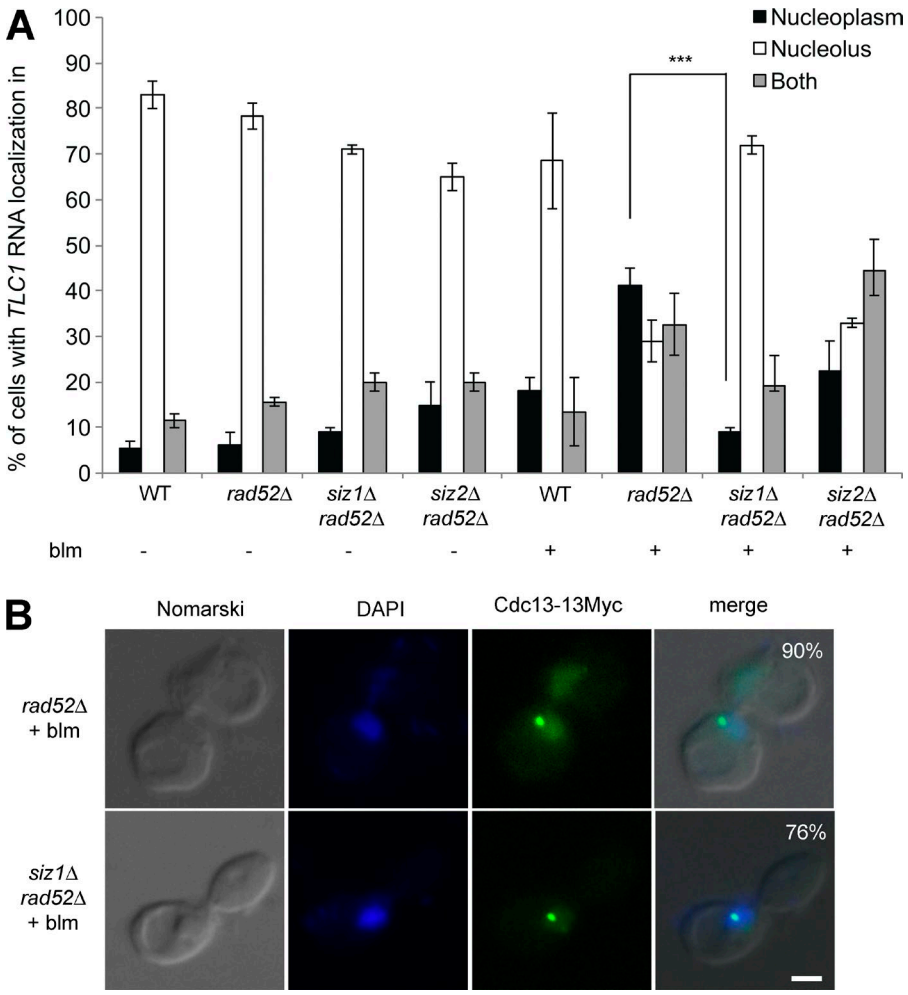

Figure 7. **The E3 SUMO ligase Siz1 is required for the accumulation of *TLC1* RNA in the nucleoplasm of *rad52Δ* cells after DNA damage.** (A) Nuclear distribution of *TLC1* RNA in various single mutants of the E3 SUMO ligases (*siz1Δ* or *siz2Δ*) in *rad52Δ* genetic background with (+) or without (–) exposure to bleomycin (blm); *n* = 200–300 cells. Error bars represent ±SD. ***, P < 0.005 (two-tailed *t* test). (B) Cdc13 clusters are still formed in the *siz1Δ rad52Δ* strain after DNA damage. Immunofluorescence (IF) analysis of Cdc13-myc was conducted in *rad52Δ* and *siz1Δ rad52Δ* cells after bleomycin (blm) treatment. Bar, 1 µm; *n* = 200 cells.

RNA focus with the Rfa1-GFP focus was detected in 27% of the cells 30 min after initiation of DNA damage (Fig. 6, D and E). At this time point, most *TLC1* RNA molecules remained outside of the DAPI-stained nucleoplasm (presumably in the nucleolus) in these cells. The colocalization between *TLC1* RNA and Rfa1-GFP increased to nearly 40% of the cells after 60 min of bleomycin treatment and remained stable afterward (Fig. 6 E).

These results could be explained by a two-step process in the accumulation of *TLC1* RNA in the nucleoplasm after DNA damage. One early step, which leads to the accumulation of a small number of *TLC1* RNA molecules at a resected DSB (Fig. 6 E), and a late step, which corresponds to the global redistribution of bulk *TLC1* RNA molecules from the nucleolus to the nucleoplasm, but not directly at DSBs (Fig. 6 C). This late redistribution may be triggered by the accumulation of unrepaired DSBs in the absence of *RAD52*. Once in the nucleoplasm, the *TLC1* RNA molecules might be associated with Cdc13 at telomeres, which would explain why in *cdc13-2* mutant, *TLC1* RNA remains in the nucleolus even in the presence of DNA damage (Figs. 4 and S4). This raises questions regarding how unrepaired DSBs could trigger this relocalization of telomerase molecules.

The E3 SUMO ligase Siz1 regulates the nucleoplasmic accumulation of *TLC1* RNA after DNA damage

The observation that *TLC1* RNA molecules are excluded from the nucleolus and accumulate in the nucleoplasm in the presence of unrepaired DSBs suggests a specific regulation of this trafficking during DNA damage. To identify regulators of the intranuclear trafficking of *TLC1* RNA, we focused on factors involved in sumoylation, a posttranslational modification that regulates DNA damage repair. Indeed, mutation or depletion of sumoylation enzymes in yeast and human cells notably results in defects in DNA repair, including recombination abnormalities and impaired DSB repair (Maeda et al., 2004; Branzei et al., 2006). Furthermore, sumoylation is known to regulate Rad52 and DSBs nuclear distribution in yeast (Torres-Rosell et al., 2007). In budding yeast, three mitotic SUMO E3 ligases have been identified, including two homologous Siz proteins (Siz1 and Siz2) and the Mms21 subunit of the essential Smc5/6 complex (Johnson and Gupta, 2001; Zhao and Blobel, 2005). Several factors involved in telomere maintenance are known to be sumoylated, including Cdc13, which is a substrate of both Siz1 and Siz2 (Hang et al., 2011). Interestingly, Cdc13 sumoylation increases after DNA damage, suggesting that Cdc13 activity may be regulated by SUMO during DNA damage (Hang et al., 2011).

To determine if sumoylation regulates the spatial distribution of telomerase after DNA damage, *TLC1* RNA localization was determined in a single mutant of two SUMO E3 ligases, *siz1Δ* and *siz2Δ*, in a *rad52Δ* background after treatment with bleomycin. In the absence of DNA damage, deletion of either *SIZ1* or *SIZ2* had no effect on the localization of *TLC1* RNA to the nucleolus in G2/M (Fig. 7 A), suggesting

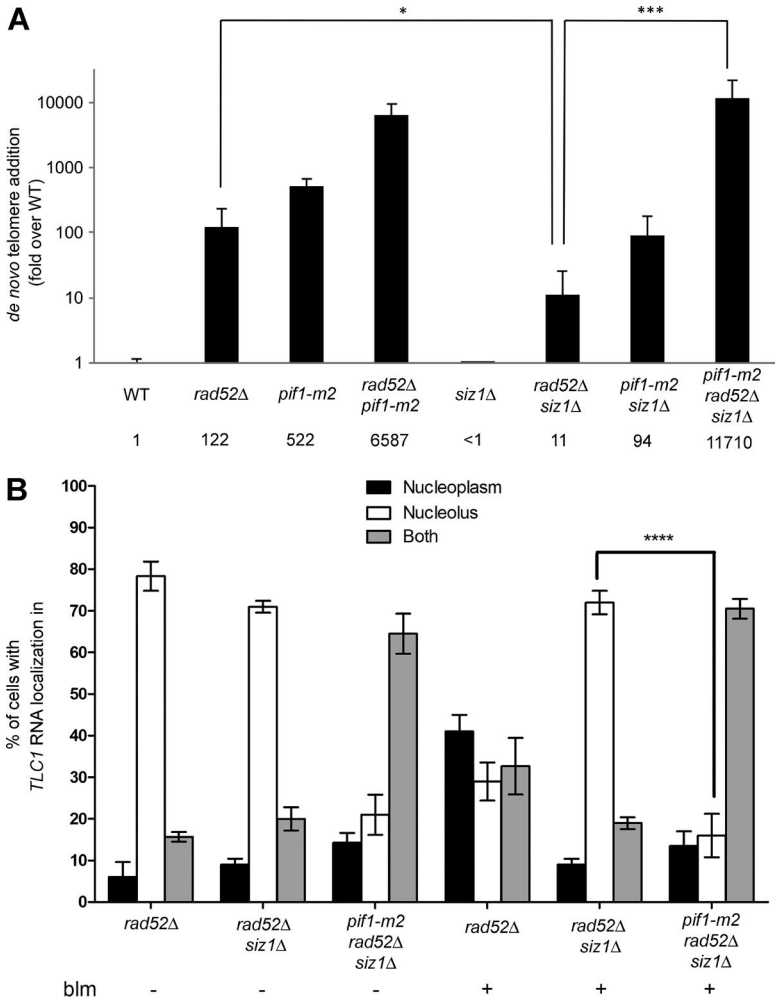

Figure 8. **Siz1 promotes de novo telomere addition in *rad52Δ* cells.** (A) Quantification of de novo telomere addition events. Values are reported as fold over wild-type (WT). *n* = 9–34 cultures. Error bars represent ± 95% confidence interval. *, P < 0.05; ***, P < 0.005 (Mann–Whitney *t* test). (B) The *pif1-m2* mutant reduces the nucleolar accumulation of *TLC1* RNA in *rad52Δ siz1Δ* cells. Nuclear distribution of *TLC1* RNA in *rad52Δ*, *siz1Δ rad52Δ*, and *pif1-m2 siz1Δ rad52Δ* cells, with (+) or without (–) exposure to bleomycin (blm). Error bars represent ±SD; *n* = 200–300 cells. ****, P < 0.0001 (two-tailed *t* test).

that these SUMO E3 ligases do not regulate the cell cycle–dependent trafficking of *TLC1* RNA. Interestingly, during bleomycin-induced DNA damage, the deletion of *SIZ1*, but not *SIZ2*, strongly decrease the nucleoplasmic accumulation of *TLC1* RNA in a *rad52Δ* strain (Fig. 7 A). These results show that Siz1, but not Siz2, controls the spatial distribution of *TLC1* RNA after DNA damage.

One trivial explanation could be that Siz1 indirectly affects the trafficking of *TLC1* RNA by modulating the processing of DSBs. To determine if Siz1 plays a role in the resection of DSBs, the kinetic of resection of a single HO cut site was measured in *rad52Δ* and *siz1Δrad52Δ* strains. No difference in the kinetic of DSB resection was observed in the absence of Siz1 (Fig. S5, A and B). Also, after DNA damage, we found that deletion of *SIZ1* did not affect the formation of Rfa1-GFP foci, a marker of DSB resection (Fig. S5 C). To identify where Siz1 acts in the DNA repair pathway, serial dilutions of *siz1Δ*, *siz2Δ*, *rad52Δ*, and double-mutant *siz1Δrad52Δ* and *siz2Δrad52Δ* strains were spotted on plates containing different concentrations of bleomycin. Unlike *SIZ2*, deletion of *SIZ1* increased the sensitivity of yeasts to bleomycin, although only at a higher concentration compared with a *RAD52* deletion (Fig. S5 D). Interestingly, the *siz1Δrad52Δ* strain showed the same sensitivity to bleomycin as a *rad52Δ* strain, showing that *RAD52* is epistatic to *SIZ1*. These results suggest that Siz1 acts downstream of Rad52 in the DNA repair pathway.

Because Siz1 is known to promote Cdc13 sumoylation after DNA damage (Hang et al., 2011), it may regulate Cdc13 clustering at DSBs and subsequent *TLC1* RNA trafficking during DNA damage. To test this hypothesis, IF on Cdc13-myc was performed in *siz1Δrad52Δ* and *rad52Δ* strains after bleomycin treatment. Cdc13 clusters and foci still formed in the *siz1Δ rad52Δ* strain as in *rad52Δ* cells (Fig. 7 B). Altogether, these results show that Siz1 is not involved in DSBs processing or Cdc13 accumulation at resected DSB but acts downstream of this process.

Siz1 promotes de novo telomere addition in the absence of *RAD52*

One key question is whether this cell cycle–dependent *TLC1* RNA trafficking plays a role in de novo telomere addition at spontaneous DSBs. To answer this question, we used the GCR assay developed by the Kolodner laboratory (Chen and Kolodner, 1999). In this assay, two counterselectable markers (*URA3* and *CAN1*) are inserted near the left telomere of chromosome V. Cells that undergo a GCR event (i.e., telomere addition, translocation) that leads to simultaneous loss of *CAN1* and *URA3* can be selected by growth on medium containing 5-FOA and canavanine. Afterward, the number of GCR events corresponding to telomere healing was quantified. The GCR assay was first performed in *rad52Δ*, *pif1-m2*, and *pif1-m2 rad52Δ* strains. As previously reported (Myung et al., 2001), deletion of *RAD52* or the *pif1-m2* mutation increase telomere healing rates (Fig. 8 A).

A

Strain	WT	*pif1-m2*	WT	*pif1-m2*	*rad52Δ*	*rad52Δ siz1Δ*
Bleomycin	-	-	+	+	+	+
total sequences	12 755 663	18 034 026	19 960 360	22 546 514	7 959 999	7 838 706
Genome coverage (x)	188	266	294	332	117	116
De novo telomere addition events	2	1	6	52	7	5
De novo telomere addition events per million reads	0,16	0,06	0,30	2,31	0,88	0,64

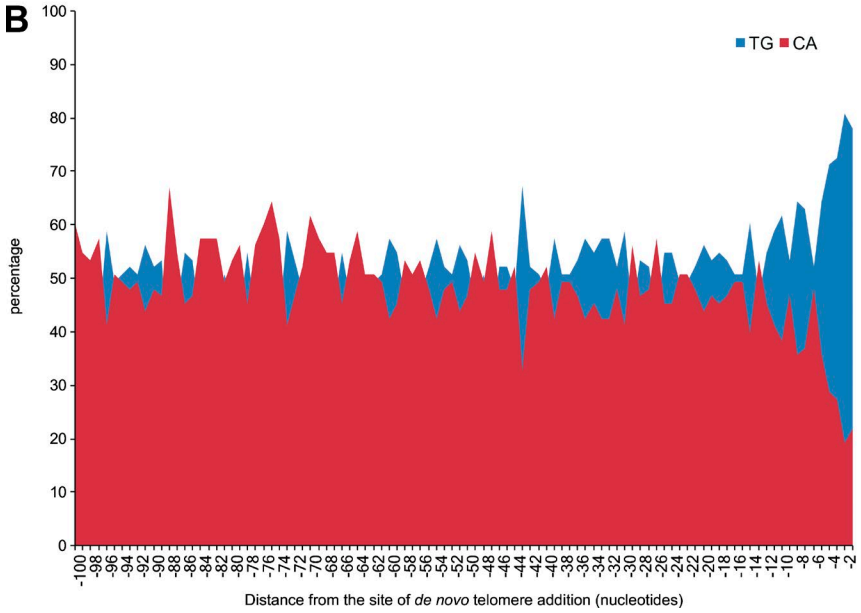

Figure 9. **Identification of telomere healing events in bleomycin-treated cells.** (A) Analysis of reads containing de novo telomere events. (B) Percentage of T+G (blue) and C+A (red) nucleotides at each position within the 100 nt upstream of the site of de novo telomere addition.

Combining the *pif1-m2* mutation with a *rad52* deletion results in a 12-fold increase in de novo telomere addition compared with the *pif1-m2* strain, as previously shown (Myung et al., 2001).

Deletion of *SIZ1* decreases the accumulation of *TLC1* RNA in the nucleoplasm of *rad52Δ* cells after DNA damage (Fig. 6 A), which should reduce de novo telomere addition and GCR rates observed in a *rad52Δ* strain. In fact, an 11-fold reduction in telomere healing rates was observed in a *siz1Δrad52Δ* strain compared with the *rad52Δ* strain (Fig. 8 A). Because Pif1 is required to promote *TLC1* RNA trafficking to the nucleolus, our model predicts that inhibition of Pif1 should suppress the nucleolar accumulation of *TLC1* RNA observed in the *siz1Δrad52Δ* strain and increase GCR rates. Indeed, the *pif1-m2* mutation partially suppresses the nucleolar accumulation of *TLC1* in the *rad52Δ siz1Δ* mutant, as *TLC1* RNA molecules accumulate in both nucleoplasm and nucleolus in the triple mutant *pif1-m2 siz1Δ rad52Δ*, with or without bleomycin treatment (Fig. 8 B). Deletion of *SIZ1* in the *pif1-m2* strain reduces GCR rates by sixfold, close to the twofold reduction previously reported for this double mutant (see Fig. 8 A). This could be because Pif1 is sumoylated during DNA damage (Hang et al., 2011), and the absence of Siz1 may affect the activity of Pif1 at sites of DNA damage. Strikingly, the triple mutant *pif1-m2 siz1Δ rad52Δ* restores the telomere healing rate to levels similar to the *pif1-m2 rad52Δ* strain (Fig. 8 A), which is consistent with our model that mutation in Pif1 bypasses the need for Siz1 activity for de novo telomere addition in *rad52Δ* cells.

Identification of telomere healing events in bleomycin treated cells

Although the GCR assay shows that Pif1, Rad52, and Siz1 regulate the frequency of telomere healing events, it remains unclear if de novo telomere addition really occurs in bleomycin-treated cells. To identify de novo telomere events in cells treated with bleomycin, WT, *pif1-m2*, *rad52Δ*, and *rad52Δ siz1Δ* cells were synchronized in G2/M with nocodazole prior treatment with bleomycin for 3 h. Genomic DNA was extracted and submitted to paired-end Illumina sequencing. Analysis of Illumina paired reads identified 73 reads containing de novo telomere events (Fig. 9 A and Table S3). 96% of these reads were identified in bleomycin-treated cells, and only three reads were identified from untreated cells, suggesting that these reads are not sequencing artifacts. Although this analysis most likely underestimates the occurrence of de novo telomere addition (see Materials and methods for details), more telomere healing events were identified per million reads in *pif1-m2*, *rad52Δ*, and *rad52Δ siz1Δ* cells treated with bleomycin compared with WT treated cells.

Telomere healing events were observed on most chromosomes (Table S3). Surprisingly, 14% of the telomere healing events identified occurred in the rDNA locus on chromosome 12, which is close to the percentage of the yeast genome occupied by this locus (~11%). Analysis of the sequences upstream de novo telomere addition events revealed the absence of nucleotide insertions or deletions, which is a feature of nonhomologous end joining and microhomology-mediated end joining repair (Sfeir and Symington, 2015). However, a TG-rich bias in the 10 nt upstream of the telomere addition sites was observed (Fig. 9 B), which was also previously reported for telomerase-dependent de novo telomere events (Putnam et al., 2004). Finally, the majority of these reads were found in the *pif1-m2* strain, suggesting that these events are mediated by telomerase activity.

Discussion

In this study, we used single-molecule imaging to study *TLC1* RNA trafficking during the cell cycle and after induction of

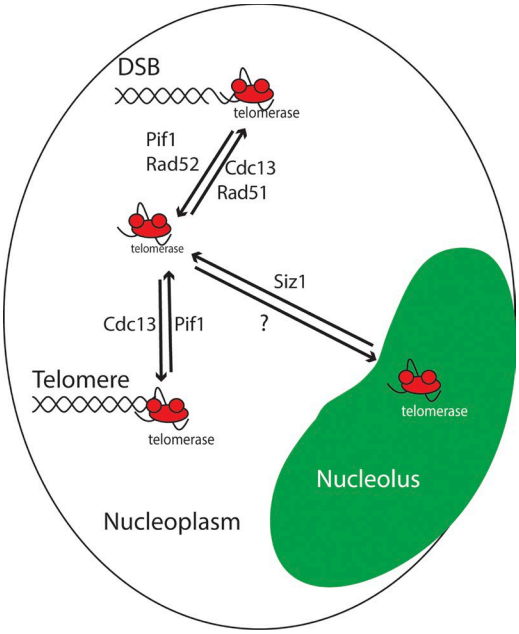

Figure 10. **Model for telomerase trafficking in G2/M and at DNA damage sites.** In the nucleoplasm, Pif1 activity removes telomerase from telomeres and promotes its accumulation in the nucleolus via an unknown mechanism. In the presence of DSBs, Pif1, and Rad52 inhibit the accumulation of telomerase and Cdc13, respectively, at break sites, leading to the accumulation of telomerase in the nucleolus and a reduction in de novo telomere addition. In the presence of DSBs, Siz1 is required for telomerase trafficking out of the nucleolus and for de novo telomere addition in *rad52Δ* cells.

DNA damage. Our results demonstrate that *TLC1* RNA, the limiting component of yeast telomerase, is engaged in an intranuclear trafficking during the cell cycle. In G1/S, *TLC1* RNA molecules are present in the nucleoplasm, whereas in G2/M, they accumulate predominantly in the nucleolus. We also show that this trafficking depends on the helicase Pif1 and is linked to the presence of DNA damage. In addition to Pif1, the key recombination protein Rad52 strongly controls this trafficking in the presence of DNA damage, as it specifically suppresses the accumulation of *TLC1* RNA molecules in the nucleoplasm and at DSBs generated by bleomycin by antagonizing the accumulation of Cdc13 at DNA breaks (Fig. 10).

However, the effect of a *RAD52* deletion on the accumulation of Cdc13 at DSBs may not be simply caused by the accumulation of longer resected DNA in this mutant, because the deletion of *RAD51*, which also produces long ssDNA at DSBs (Sugawara et al., 1995; Zhu et al., 2008), completely abolishes the formation of Cdc13 foci. Interestingly, deletion of *RAD51* suppresses the effect of a *RAD52* deletion on *TLC1* RNA trafficking. This result supports a previous observation that Rad51 is required for the recruitment of Cdc13 and Est2 to a nonrepairable DSB (Oza et al., 2009). Why Rad52 and Rad51 have opposite effects on the formation of Cdc13 foci is still unclear.

Using Illumina paired-end sequencing, we identified several reads containing de novo telomere addition events in the genome of yeasts treated with bleomycin. De novo telomere addition occurred downstream of TG-rich sequences less than 10 nt. A recent characterization of an endogenous hotspot of de novo telomere addition in yeast revealed a bipartite structure, with a TG-rich core sequence where telomere addition occurs, and an upstream proximal Stim sequence that binds Cdc13 and stimulates telomere addition (Obodo et al., 2016). Interestingly, de novo telomere addition is increased at this bipartite hotspot in the absence of Rad52. Hence, because of their short TG-rich core sequence, it is possible that several of the sites of de novo telomere addition identified in the DNA-sequencing study may contain this bipartite structure. Another surprising result is that 14% of the reads containing de novo telomeres were from the rDNA locus, suggesting the presence of telomerase activity in the nucleolus. Because DSBs in rDNA in yeast are processed in the nucleolus but repaired by HR in the nucleoplasm (Torres-Rosell et al., 2007), the unusual dynamics of these DSBs between the nucleolus and the nucleoplasm may explain in part their accessibility to telomerase activity in the nucleoplasm.

In addition, we demonstrate that the E3 SUMO ligase Siz1 regulates the spatial distribution of *TLC1* RNA after DNA damage without affecting DSB processing or Cdc13 accumulation at DSBs. DNA damage is known to trigger a wave of sumoylation leading to simultaneous multisite modifications of several DNA repair proteins of the HR pathway in yeast (Psakhye and Jentsch, 2012). However, these sumoylation events depend on the Siz2 SUMO ligase and not on Siz1, suggesting that the effect of Siz1 on *TLC1* RNA localization is independent of the main role of SUMO in the modulation of the HR pathway. Although the effect of a *SIZ1* deletion on *TLC1* RNA trafficking might be explained by the Siz1-dependent sumoylation of Cdc13 (Hang et al., 2011), this sumoylation event was shown to inhibit telomerase binding to Cdc13. Therefore, other targets of Siz1 may be involved in this process. Sumoylation by Siz1 is required for de novo telomere addition in the absence of Rad52 and, to a lesser extent, in a *pif1-m2* strain. This requirement for Siz1 activity is completely suppressed in a double *pif1-m2 rad52Δ* mutation. These data support our model that by reducing *TLC1* RNA trafficking to the nucleolus, the *pif1-m2* mutation bypasses the spatial restriction on telomerase access to DNA breaks observed in the *siz1Δ rad52Δ* strain (Fig. 10).

In line with the observation that DNA repair is excluded from the nucleolus (Dion et al., 2013), our study reveals how the spatial segregation of telomerase and HR activities restricts telomerase access to DSBs. This process is not specific to budding yeast telomerase, because the catalytic subunit of human telomerase (hTERT) was also shown to accumulate in the nucleolus after ionizing radiation–induced DSBs (Wong et al., 2002), indicating that nucleolar localization of telomerase after DNA damage may be a conserved process during evolution.

Materials and methods

Constructs and strains

Table S1 lists strain genotypes. Yeast strains were generated by disrupting the *RAD52*, *RAD51*, *SIZ1*, *SIZ2*, *MRE11, XRS2*, *TEL1*, or *MEC1* genes in *W303* strain by a one-step PCR disruption method using KAN marker (Wach et al., 1994). The *mec1*Δ strains were kept viable by deletion of the *SML1* gene (Zhao et al., 1998). In this strain, the KAN marker was removed by transforming cells with pSH47 expressed Cre recombinase. The *cdc13-2* strain transformed with the plasmid pVL438 *CDC13* (Ycp33 CEN, *URA3*, and *CDC13*; Chandra et al., 2001) was obtained from R. Wellinger's laboratory (Université de Sherbrooke, Sherbrooke, Canada). Deletion of *RAD52* was followed by the elimination of the pVL438 *CDC13* plasmid using 5-FOA. Strains carrying Rfa1-GFP, Rfa1-mCherry, Cdc13-GFP, and Cdc13-13Myc allele at the *RFA1* and *CDC13* chromosomal locus were generated by a PCR one-step tagging method using plasmids pFA6A-GFP-KANMX4, pFA6A-

mCherry-Kan, or pFA6A-13Myc-KANMX4 (Knop et al., 1999). Verification of these strains was performed by PCR, microscopy, and/or Western blot. For Cdc13-GFP and Cdc13-13Myc strains, senescence experiments were conducted by repeatedly streaking strains. For all these strains, the *RAD52* gene disruptions were obtained by using *TRP1*, *KAN*, or Hygro markers. *RAD51* deletion was also obtained by using *TRP1* marker.

Cell cycle–dependent localization of *TLC1* RNA and induction of DSBs

Asynchronously growing WT yeast cells (W303) were grown in YEPD (yeast extract peptone-dextrose) until OD_{600} 0.3 to 0.4, fixed with paraformaldehyde, and processed for FISH analysis to detect *TLC1* RNA and *ITS1* pre-rRNA. *ITS1* FISH probe was provided by D. Zenklusen (Université de Montréal, Montréal, Quebec, Canada). The cell cycle stage of the cells was estimated by measuring the bud-to-mother size ratio (budding index) as G1 (cells without bud), S phase (cells with small to mid-size bud), and G2/M (cells with large bud or sharing the nucleus between mother and daughter). This method is highly reproducible for scoring G2/M cells, because nearly identical percentages of *TLC1* RNA distribution were measured in nocodazole-treated cells and nontreated cells (see Fig. 2, B and C). For induction of DSBs, haploid WT and *rad52Δ* strains were grown in YEPD medium (at OD_{600} ∼0.2) and exposed to 5 µg/ml of bleomycin (BLE011.10; Bioshop) for 180 min. In these conditions, 90% of the cells have at least one DSB after 180 min (Fig. S2). The presence and number of DNA damage per cell after bleomycin treatment were quantified using the number of γ-H2A foci, which correlates with the number of DSBs per cell (Sedelnikova et al., 2002). For nocodazole treatment, WT and *rad52Δ* cells were grown in YEPD medium to OD_{600} ∼0.2 before addition of 15 µg/ml nocodazole for 90 min, and synchronization of cells in G2/M was monitored by microscopy. In these conditions, more than 90% of cells are in G2/M. 5 µg/ml bleomycin was then added, and cells were incubated for another 180 min.

FISH and IF

The yeast fixation protocol and fluorescent in situ hybridization to detect endogenous *TLC1* RNA have been described previously (Pfingsten et al., 2012). Five Cy3-labeled 50-nt probes were used to detect the endogenous *TLC1* RNA, and one Cy5-labeled 50-nt probe was used to detect the *ITS1* pre-rRNA. For colocalization experiments with endogenous Rfa1-GFP, yeast was cultured at room temperature, and fixation was performed in 1× PBS, pH 7.4, to preserve GFP fluorescence. Dual FISH-IF or IF-only protocols were conducted as described previously (Gallardo and Chartrand, 2011). In brief, after the last wash of 1× SSC of the FISH protocol, spheroplasts were incubated in 1× PBS containing 0.1% BSA, 1× PBS containing 0.1% BSA and 0.1% NP40, and 1× PBS containing 0.1% BSA for 2 min each at room temperature. The primary antibodies used to detect γ-H2A (18255; Abcam) or myc epitope (9E10; Roche) were diluted to 1:5,000 and 1:400, respectively, in 1× PBS containing 0.1% BSA, 20 mM VRC, and 120 U/ml RNA Guard and incubated for 2 h at 37°C. Spheroplasts were washed with 1× PBS containing 0.1% BSA, 1× PBS containing 0.1% BSA and 0.1% NP-40, and 1× PBS containing 0.1% BSA for 2 min each at room temperature. The secondary antibody (Alexa Fluor 488 conjugate) was diluted to 1:1,000 in 1× PBS containing 0.1% BSA, 20 mM VRC, and 120 U/ml RNA Guard, and incubated 1h in the dark at room temperature. Finally, cells were washed in 1× PBS containing 0.1% BSA, 1× PBS containing 0.1% BSA and 0.1% NP-40, and 1× PBS 0.1% BSA for 1 min each at room temperature. The coverslips were incubated in 1× PBS containing DAPI before mounting on slides.

Image acquisition, deconvolution, and processing

All images were acquired using an Axio Imager 2 epifluorescence upright microscope (ZEISS) equipped with a 100× differential interference contrast (DIC) H (1.4 NA) objective and a Photometrics CoolSNAP fx CCD camera. Endogenous *TLC1* RNA foci were detected using Cy3.0 filter, *ITS1* probe was detected using Cy5.0 filter, and Rfa1-GFP or γ-H2A were detected using a FITC filter. Image acquisition times for DIC, DAPI, *TLC1* RNA, and *ITS1* pre-rRNA were 40, 20, 1,600, and 800 ms, respectively. Images were acquired and processed with ZEISS software or deconvolved by Autoquant X3 software using a theoretical PSF algorithm and analyzed using Metamorph software. 100 fields of yeast cells were acquired as Z stacks of 14 planes minimum, with 0.5 µm between planes in the Z axis. Inspection of all focal planes of each cell was performed to quantify colocalization between *TLC1* RNA, *ITS1* pre-rRNA (nucleolus) or DAPI (nucleoplasm), with reproducible results obtained with two or three different individuals. For each yeast strain, a total of 200 G2/M cells were randomly scored in two biologically independent experiments. The linescan application of Fiji or Metamorph software was also used to quantify *TLC1* RNA, *ITS1* RNA, and DAPI fluorescence distribution in the nucleus of yeast cells. Numbers are expressed as percentage of cells with *TLC1* RNA located in the nucleoplasm or nucleolus or evenly distributed between both compartments. Simultaneous FISH on *TLC1* and *MDN1* RNA was performed to determine the percentage of colocalization of *TLC1* RNA foci with a random nuclear focus, represented by the *MDN1* transcription site. The *MDN1* FISH probes were provided by D. Zenklusen.

Live-cell imaging

Cells expressing fusion protein Rfa1-GFP, Cdc13-GFP, or Cdc13-GFP and Rfa1-mCherry in *rad52Δ* genetic background were incubated overnight at 25°C in 2 ml SC-TRP and then diluted to OD_{600} ∼0.2 and grown for one cell cycle. Cdc13-GFP foci and colocalization between Cdc13-GFP and Rfa1-mCherry were induced by 5 µg/ml bleomycin for 3 h. Cells were collected by centrifugation at 2,000 *g*, mounted on standard glass slides, and covered with a coverslip appropriate to the optics of the microscope. All the images were acquired using an Axio Imager 2 epifluorescence upright microscope (ZEISS) equipped with a 100× DIC H (1.4 NA) objective and an Evolve fx EM-CCD camera or microscope AXIO OBSERVER Z1 confocal spinning disk (ZEISS) equipped with the same objective and camera. For each field of cells, 11 fluorescent images at each of the relevant wavelengths were obtained at 0.4-µm intervals along the Z axis. Inspection of all focal planes of each cell was performed to quantify colocalization. Image acquisition times for DIC, bright-field, GFP, and mCherry were 40, 40, 900, and 60 ms, respectively.

Quantitative analysis of Cdc13 foci and clusters

Determination of Cdc13 focus and cluster diameter and maximal fluorescence intensity was calculated as described previously (Gallardo et al., 2011).

DSB resection assay

Yeast was grown to early–mid log phase in YEP-raffinose medium at 30°C. HO endonuclease was induced by the addiction of 3% galactose. Samples were harvested before galactose addition and every 30 min after induction for 4 h. Genomic DNA was extracted and digested by PciI restriction enzyme. DNA fragments were separated on a 1% agarose gel and transferred on a neutral nylon membrane. Southern blot was performed with a probe generated by PCR amplification of a sequence close to the HO cut site. DNA loaded at each time point was normalized using a probe against the *AGX1* gene. Intensities of bands on the Southern blot were quantified with Image Lab. Resection was measured as the ratio of the signal intensity for each time point relative to the signal intensity of the initial HO cleavage time point.

GCR assay and characterization of telomere healing events

All GCR rates were determined by fluctuation tests. Mutation rates were calculated using the median method (Putnam and Kolodner, 2010). Re-

sults shown are the mean of three to five experiments using five to seven cultures. After the GCR assay, DNA was extracted from 20 5-FOA$^+$ Can$^+$ colonies from each strain (but only eight for the WT strain). To identify the breaking point where the GCR took place, we used the approached used in (Motegi and Myung, 2007). In brief, 22 pairs of PCR primers were designed to cover the whole 12-kb region where the break could have happened to generate a 5-FOA$^+$ Can$^+$ colony. Each primer pair was designed to generate overlapping ∼600-bp amplicons. Starting from the centromere-proximal extremity, the first primer pair that did not give amplification is referred as the breaking point.

Each breaking point was further analyzed to characterize the presence of de novo telomere addition at the breaks. This analysis was performed as in (Motegi and Myung, 2007). In brief, each sample was amplified using the antisense PCR primer of the breaking point with a telomere primer (5′-CACCACACCCACACAC-3′). The antisense primer of the last working pair (flanking the breaking point) was also used with the telomere primer. Those two primer pairs served to identify de novo telomere addition. As controls, each sample was amplified using the breaking point primer pair and the last working primer pair. As a positive control, the telomere primer was used with an antisense primer that flanks the telomere 1L. Finally, one sample with a breaking point upstream of the breaking point analyzed and one downstream of it were added. Those were used as controls for the specificity of the primer pairs.

The results are displayed as a ratio of telomere healing events identified versus the number of clones characterized for each strain. Then, this ratio is applied on the spontaneous GCR rate calculated for the corresponding strain to establish a spontaneous telomere healing rate. This rate is than compared with the rate of the WT strain, which is set as 1.

Identification of telomere healing events by Illumina paired-end sequencing

Cultures were started from an OD_{600} of 0.2. When the OD_{600} reached 0.4, 15 µg/ml nocodazole was added to the culture. Cultures were incubated for 3 h until >80% of the cells were synchronized in G2/M. Synchronization was assessed by microscopy. If needed, 5 µg/ml bleomycin was added and cultures were incubated another 3 h before harvesting the cells. Genomic DNA was extracted, and 1 µg was sent for paired-end Illumina sequencing on an Illumina HiSeq2000. Each condition was done in duplicate. Genome coverage for each sample ranged from 25 to 210× (2,792,066 to 14,219,231 sequences).

Datasets were analyzed using a Galaxy (Afgan et al., 2016) modified version of a previously published workflow (Zampini et al., 2015). Sequences were filtered for a minimum length of 40 nt, an average quality of at least 20, and no more than 50 nt under a quality of 20. They were then aligned using the Burrows-Wheeler aligner against the sacCer3 reference genome (NCBI Assembly accession no. GCA_000146045.2) from which telomere sequences were removed. Read pairs for which both reads were successfully mapped do not contain de novo telomere additions and were discarded. The first 25 nt of the remaining pairs were aligned using Bowtie, and sequences which were mapped for either none or both of the paired end reads were discarded. Between 177,689 to 544,055 sequences remained for analysis in each dataset at this point. Read pairs were sorted according to the percentage of CA, CCA, and CCCA in the first 50 nt of the unmapped read. Unmapped reads with at least 24 nucleotides of telomeric repeats in their first 50 nt were then analyzed manually to identify telomere healing events. The remaining pairs were further filtered for at least 12 nt of telomeric repeats in the first 24 nt of the unmapped read and then analyzed in the same manner. Finally, to ensure that the events found were de novo telomere addition and not random addition of TG repeats, identified sequences were compared with the *TLC1* RNA template.

Although this approach allows the detection of de novo telomere additions, it most likely underestimates their occurrence. First, Illumina sequencing biases against GC-rich and GC-poor regions may translate into fewer GC-rich telomere reads. Second, telomeres were removed from the reference genome in order for telomere-containing sequences to remain unmapped, but if the first 25 nt of a telomere sequence match an internal telomeric tract (as in the subtelomeric regions), the read was discarded after a successful alignment using Bowtie. Third, because a lot of sequences in the subtelomeric regions are shared between chromosomes ends, it is difficult to assign a sequence to a specific telomere. For this reason, subtelomeric sequences (10 kb from telomeres) were ignored in the analysis. Fourth, DNA fragments with identical sequences at both ends were ignored. These pseudopalindromes are artifacts created by the presence of long ssDNA (Star et al., 2014). One library from the *rad52Δ* strain was discarded because of the presence of a very high number of reads with pseudo-palindromes, possibly because *rad52Δ* cells have longer resected DNA at DSBs. Lastly, because telomere sequences shorter than 12 nt were not analyzed, short de novo telomere additions were ignored. Fragmentation of the DNA near a site of telomere addition during library preparation therefore means that some occurrences were missed.

Statistical analysis

A two-tailed Student's *t* test or analysis of variance was used to calculate the statistical significance. A Mann–Whitney *t* test was used for the GCR assay. Statistical significance was defined as $P < 0.05$ (*). Calculations were performed using GraphPad.

Online supplemental material

Fig. S1 presents *TLC1* RNA localization in *pif1Δ* and *pif1-m2* strains. Fig. S2 describes quantification of γ-H2A foci and cell cycle synchronization. Fig. S3 shows the analysis of *TLC1* RNA colocalization with DSBs. Fig. S4 presents a quantitative analysis of Cdc13 foci. Fig. S5 shows that Siz1 is not involved in DSBs processing but acts downstream of Rad52 in DNA repair. Table S1 shows all yeast strains genotypes. Table S2 lists p-values of all the strains tested in Fig. 4 B. Table S3 lists all the de novo telomere addition identified by DNA sequencing.

Acknowledgments

The authors thank R. Wellinger, J. Cobb, R. Kolodner, D. Durocher, and L. Symington for yeast strains and D. Zenklusen (Université de Montréal) for the *ITS1* and *MDN1* FISH probes. We also thank R. Wellinger, L. Harrington, E. Querido, and M. Hendzel for critical reading of the manuscript.

This project was supported by a grant from the Canadian Institutes of Health Research (MOP-89768). M. Lalonde is supported by a fellowship from the Fonds de Recherche du Québec-Santé. F. Gallardo was supported by a doctoral fellowship from the Terry Fox Foundation. G. Morin and H. Laprade were supported by a Natural Sciences and Engineering Research Council of Canada CDMC-CREATE fellowship. P. Chartrand holds a Fonds de Recherche du Québec-Santé Research Chair.

The authors declare no competing financial interests.

Author contributions: F. Ouenzar, M. Lalonde, and F. Gallardo performed FISH and IF experiments, analyzed microscopy data, and prepared strains. G. Morin helped to perform the FISH experiments shown in Fig 4. M. Lalonde prepared strains and performed GCR assays and analysis of Illumina sequencing. H. Laprade performed GCR assays and DNA resection. S. Tremblay-Belzile helped with bioinformatics analysis. F. Ouenzar, M. Lalonde, and P. Chartrand designed the experiments and wrote the paper.

Submitted: 21 October 2016
Revised: 21 April 2017
Accepted: 18 May 2017

References

Afgan, E., D. Baker, M. van den Beek, D. Blankenberg, D. Bouvier, M. Čech, J. Chilton, D. Clements, N. Coraor, C. Eberhard, et al. 2016. The Galaxy platform for accessible, reproducible and collaborative biomedical analyses: 2016 update. *Nucleic Acids Res.* 44(W1):W3–W10. http://dx.doi.org/10.1093/nar/gkw343

Alani, E., R. Thresher, J.D. Griffith, and R.D. Kolodner. 1992. Characterization of DNA-binding and strand-exchange stimulation properties of y-RPA, a yeast single-strand-DNA-binding protein. *J. Mol. Biol.* 227:54–71. http://dx.doi.org/10.1016/0022-2836(92)90681-9

Bajon, E., N. Laterreur, and R.J. Wellinger. 2015. A single templating RNA in yeast telomerase. *Cell Reports.* 12:441–448. http://dx.doi.org/10.1016/j.celrep.2015.06.045

Barlow, J.H., M. Lisby, and R. Rothstein. 2008. Differential regulation of the cellular response to DNA double-strand breaks in G1. *Mol. Cell.* 30:73–85. http://dx.doi.org/10.1016/j.molcel.2008.01.016

Bianchi, A., and D. Shore. 2008. How telomerase reaches its end: mechanism of telomerase regulation by the telomeric complex. *Mol. Cell.* 31:153–165. http://dx.doi.org/10.1016/j.molcel.2008.06.013

Bianchi, A., S. Negrini, and D. Shore. 2004. Delivery of yeast telomerase to a DNA break depends on the recruitment functions of Cdc13 and Est1. *Mol. Cell.* 16:139–146. http://dx.doi.org/10.1016/j.molcel.2004.09.009

Branzei, D., J. Sollier, G. Liberi, X. Zhao, D. Maeda, M. Seki, T. Enomoto, K. Ohta, and M. Foiani. 2006. Ubc9- and mms21-mediated sumoylation counteracts recombinogenic events at damaged replication forks. *Cell.* 127:509–522. http://dx.doi.org/10.1016/j.cell.2006.08.050

Chandra, A., T.R. Hughes, C.I. Nugent, and V. Lundblad. 2001. Cdc13 both positively and negatively regulates telomere replication. *Genes Dev.* 15:404–414. http://dx.doi.org/10.1101/gad.861001

Chen, C., and R.D. Kolodner. 1999. Gross chromosomal rearrangements in *Saccharomyces cerevisiae* replication and recombination defective mutants. *Nat. Genet.* 23:81–85. http://dx.doi.org/10.1038/12687

Chen, J., and J. Stubbe. 2005. Bleomycins: Towards better therapeutics. *Nat. Rev. Cancer.* 5:102–112. http://dx.doi.org/10.1038/nrc1547

Chung, W.H., Z. Zhu, A. Papusha, A. Malkova, and G. Ira. 2010. Defective resection at DNA double-strand breaks leads to de novo telomere formation and enhances gene targeting. *PLoS Genet.* 6:e1000948. http://dx.doi.org/10.1371/journal.pgen.1000948

Counter, C.M., M. Meyerson, E.N. Eaton, and R.A. Weinberg. 1997. The catalytic subunit of yeast telomerase. *Proc. Natl. Acad. Sci. USA.* 94:9202–9207. http://dx.doi.org/10.1073/pnas.94.17.9202

Diede, S.J., and D.E. Gottschling. 1999. Telomerase-mediated telomere addition in vivo requires DNA primase and DNA polymerases alpha and delta. *Cell.* 99:723–733. http://dx.doi.org/10.1016/S0092-8674(00)81670-0

Dion, V., V. Kalck, A. Seeber, T. Schleker, and S.M. Gasser. 2013. Cohesin and the nucleolus constrain the mobility of spontaneous repair foci. *EMBO Rep.* 14:984–991. http://dx.doi.org/10.1038/embor.2013.142

Frank, C.J., M. Hyde, and C.W. Greider. 2006. Regulation of telomere elongation by the cyclin-dependent kinase CDK1. *Mol. Cell.* 24:423–432. http://dx.doi.org/10.1016/j.molcel.2006.10.020

Gallardo, F., and P. Chartrand. 2011. Visualizing mRNAs in fixed and living yeast cells. *Methods Mol. Biol.* 714:203–219. http://dx.doi.org/10.1007/978-1-61779-005-8_13

Gallardo, F., C. Olivier, A.T. Dandjinou, R.J. Wellinger, and P. Chartrand. 2008. TLC1 RNA nucleo-cytoplasmic trafficking links telomerase biogenesis to its recruitment to telomeres. *EMBO J.* 27:748–757. http://dx.doi.org/10.1038/emboj.2008.21

Gallardo, F., N. Laterreur, E. Cusanelli, F. Ouenzar, E. Querido, R.J. Wellinger, and P. Chartrand. 2011. Live cell imaging of telomerase RNA dynamics reveals cell cycle-dependent clustering of telomerase at elongating telomeres. *Mol. Cell.* 44:819–827. http://dx.doi.org/10.1016/j.molcel.2011.09.020

Gasior, S.L., A.K. Wong, Y. Kora, A. Shinohara, and D.K. Bishop. 1998. Rad52 associates with RPA and functions with rad55 and rad57 to assemble meiotic recombination complexes. *Genes Dev.* 12:2208–2221. http://dx.doi.org/10.1101/gad.12.14.2208

Hang, L.E., X. Liu, I. Cheung, Y. Yang, and X. Zhao. 2011. SUMOylation regulates telomere length homeostasis by targeting Cdc13. *Nat. Struct. Mol. Biol.* 18:920–926. http://dx.doi.org/10.1038/nsmb.2100

Ira, G., A. Pellicioli, A. Balijja, X. Wang, S. Fiorani, W. Carotenuto, G. Liberi, D. Bressan, L. Wan, N.M. Hollingsworth, et al. 2004. DNA end resection, homologous recombination and DNA damage checkpoint activation require CDK1. *Nature.* 431:1011–1017. http://dx.doi.org/10.1038/nature02964

Johnson, E.S., and A.A. Gupta. 2001. An E3-like factor that promotes SUMO conjugation to the yeast septins. *Cell.* 106:735–744. http://dx.doi.org/10.1016/S0092-8674(01)00491-3

Knop, M., K. Siegers, G. Pereira, W. Zachariae, B. Winsor, K. Nasmyth, and E. Schiebel. 1999. Epitope tagging of yeast genes using a PCR-based strategy: more tags and improved practical routines. *Yeast.* 15(10B):963–972. http://dx.doi.org/10.1002/(SICI)1097-0061(199907)15:10B<963::AID-YEA399>3.0.CO;2-W

Kramer, K.M., and J.E. Haber. 1993. New telomeres in yeast are initiated with a highly selected subset of TG1-3 repeats. *Genes Dev.* 7(12a, 12A):2345–2356. http://dx.doi.org/10.1101/gad.7.12a.2345

Krogh, B.O., and L.S. Symington. 2004. Recombination proteins in yeast. *Annu. Rev. Genet.* 38:233–271. http://dx.doi.org/10.1146/annurev.genet.38.072902.091500

Lingner, J., T.R. Hughes, A. Shevchenko, M. Mann, V. Lundblad, and T.R. Cech. 1997. Reverse transcriptase motifs in the catalytic subunit of telomerase. *Science.* 276:561–567. http://dx.doi.org/10.1126/science.276.5312.561

Lisby, M., U.H. Mortensen, and R. Rothstein. 2003. Colocalization of multiple DNA double-strand breaks at a single Rad52 repair centre. *Nat. Cell Biol.* 5:572–577. http://dx.doi.org/10.1038/ncb997

Lydeard, J.R., Z. Lipkin-Moore, S. Jain, V.V. Eapen, and J.E. Haber. 2010. Sgs1 and exo1 redundantly inhibit break-induced replication and de novo telomere addition at broken chromosome ends. *PLoS Genet.* 6:e1000973. http://dx.doi.org/10.1371/journal.pgen.1000973

Maeda, D., M. Seki, F. Onoda, D. Branzei, Y. Kawabe, and T. Enomoto. 2004. Ubc9 is required for damage-tolerance and damage-induced interchromosomal homologous recombination in *S. cerevisiae*. *DNA Repair (Amst.).* 3:335–341. http://dx.doi.org/10.1016/j.dnarep.2003.11.011

Makovets, S., and E.H. Blackburn. 2009. DNA damage signalling prevents deleterious telomere addition at DNA breaks. *Nat. Cell Biol.* 11:1383–1386. http://dx.doi.org/10.1038/ncb1985

Mangahas, J.L., M.K. Alexander, L.L. Sandell, and V.A. Zakian. 2001. Repair of chromosome ends after telomere loss in *Saccharomyces*. *Mol. Biol. Cell.* 12:4078–4089. http://dx.doi.org/10.1091/mbc.12.12.4078

Martina, M., M. Clerici, V. Baldo, D. Bonetti, G. Lucchini, and M.P. Longhese. 2012. A balance between Tel1 and Rif2 activities regulates nucleolytic processing and elongation at telomeres. *Mol. Cell. Biol.* 32:1604–1617. http://dx.doi.org/10.1128/MCB.06547-11

Mazumder, A., K. Tummler, M. Bathe, and L.D. Samson. 2013. Single-cell analysis of ribonucleotide reductase transcriptional and translational response to DNA damage. *Mol. Cell. Biol.* 33:635–642. http://dx.doi.org/10.1128/MCB.01020-12

McGee, J.S., J.A. Phillips, A. Chan, M. Sabourin, K. Paeschke, and V.A. Zakian. 2010. Reduced Rif2 and lack of Mec1 target short telomeres for elongation rather than double-strand break repair. *Nat. Struct. Mol. Biol.* 17:1438–1445. http://dx.doi.org/10.1038/nsmb.1947

Moore, J.K., and J.E. Haber. 1996. Cell cycle and genetic requirements of two pathways of nonhomologous end-joining repair of double-strand breaks in *Saccharomyces cerevisiae*. *Mol. Cell. Biol.* 16:2164–2173. http://dx.doi.org/10.1128/MCB.16.5.2164

Motegi, A., and K. Myung. 2007. Measuring the rate of gross chromosomal rearrangements in *Saccharomyces cerevisiae*: A practical approach to study genomic rearrangements observed in cancer. *Methods.* 41:168–176. http://dx.doi.org/10.1016/j.ymeth.2006.07.025

Mozdy, A.D., and T.R. Cech. 2006. Low abundance of telomerase in yeast: Implications for telomerase haploinsufficiency. *RNA.* 12:1721–1737. http://dx.doi.org/10.1261/rna.134706

Myung, K., C. Chen, and R.D. Kolodner. 2001. Multiple pathways cooperate in the suppression of genome instability in *Saccharomyces cerevisiae*. *Nature.* 411:1073–1076. http://dx.doi.org/10.1038/35082608

Nugent, C.I., T.R. Hughes, N.F. Lue, and V. Lundblad. 1996. Cdc13p: a single-strand telomeric DNA-binding protein with a dual role in yeast telomere maintenance. *Science.* 274:249–252. http://dx.doi.org/10.1126/science.274.5285.249

Obodo, U.C., E.A. Epum, M.H. Platts, J. Seloff, N.A. Dahlson, S.M. Velkovsky, S.R. Paul, and K.L. Friedman. 2016. Endogenous hot spots of de novo telomere addition in the yeast genome contain proximal enhancers that bind Cdc13. *Mol. Cell. Biol.* 36:1750–1763. http://dx.doi.org/10.1128/MCB.00095-16

Oza, P., S.L. Jaspersen, A. Miele, J. Dekker, and C.L. Peterson. 2009. Mechanisms that regulate localization of a DNA double-strand break to

the nuclear periphery. *Genes Dev.* 23:912–927. http://dx.doi.org/10.1101/gad.1782209

Pâques, F., and J.E. Haber. 1999. Multiple pathways of recombination induced by double-strand breaks in *Saccharomyces cerevisiae*. *Microbiol. Mol. Biol. Rev.* 63:349–404.

Pennaneach, V., C.D. Putnam, and R.D. Kolodner. 2006. Chromosome healing by de novo telomere addition in *Saccharomyces cerevisiae*. *Mol. Microbiol.* 59:1357–1368. http://dx.doi.org/10.1111/j.1365-2958.2006.05026.x

Pennock, E., K. Buckley, and V. Lundblad. 2001. Cdc13 delivers separate complexes to the telomere for end protection and replication. *Cell.* 104:387–396. http://dx.doi.org/10.1016/S0092-8674(01)00226-4

Pfingsten, J.S., K.J. Goodrich, C. Taabazuing, F. Ouenzar, P. Chartrand, and T.R. Cech. 2012. Mutually exclusive binding of telomerase RNA and DNA by Ku alters telomerase recruitment model. *Cell.* 148:922–932. http://dx.doi.org/10.1016/j.cell.2012.01.033

Phillips, J.A., A. Chan, K. Paeschke, and V.A. Zakian. 2015. The pif1 helicase, a negative regulator of telomerase, acts preferentially at long telomeres. *PLoS Genet.* 11:e1005186. http://dx.doi.org/10.1371/journal.pgen.1005186

Psakhye, I., and S. Jentsch. 2012. Protein group modification and synergy in the SUMO pathway as exemplified in DNA repair. *Cell.* 151:807–820. http://dx.doi.org/10.1016/j.cell.2012.10.021

Putnam, C.D., and R.D. Kolodner. 2010. Determination of gross chromosomal rearrangement rates. *Cold Spring Harb. Protoc.* 2010:t5492. http://dx.doi.org/10.1101/pdb.prot5492

Putnam, C.D., V. Pennaneach, and R.D. Kolodner. 2004. Chromosome healing through terminal deletions generated by de novo telomere additions in *Saccharomyces cerevisiae*. *Proc. Natl. Acad. Sci. USA.* 101:13262–13267. http://dx.doi.org/10.1073/pnas.0405443101

Raderschall, E., E.I. Golub, and T. Haaf. 1999. Nuclear foci of mammalian recombination proteins are located at single-stranded DNA regions formed after DNA damage. *Proc. Natl. Acad. Sci. USA.* 96:1921–1926. http://dx.doi.org/10.1073/pnas.96.5.1921

Ribaud, V., C. Ribeyre, P. Damay, and D. Shore. 2012. DNA-end capping by the budding yeast transcription factor and subtelomeric binding protein Tbf1. *EMBO J.* 31:138–149. http://dx.doi.org/10.1038/emboj.2011.349

Ribeyre, C., and D. Shore. 2013. Regulation of telomere addition at DNA double-strand breaks. *Chromosoma.* 122:159–173. http://dx.doi.org/10.1007/s00412-013-0404-2

Ricchetti, M., B. Dujon, and C. Fairhead. 2003. Distance from the chromosome end determines the efficiency of double strand break repair in subtelomeres of haploid yeast. *J. Mol. Biol.* 328:847–862. http://dx.doi.org/10.1016/S0022-2836(03)00315-2

Rogakou, E.P., C. Boon, C. Redon, and W.M. Bonner. 1999. Megabase chromatin domains involved in DNA double-strand breaks in vivo. *J. Cell Biol.* 146:905–916. http://dx.doi.org/10.1083/jcb.146.5.905

Schulz, V.P., and V.A. Zakian. 1994. The saccharomyces PIF1 DNA helicase inhibits telomere elongation and de novo telomere formation. *Cell.* 76:145–155. http://dx.doi.org/10.1016/0092-8674(94)90179-1

Sedelnikova, O.A., E.P. Rogakou, I.G. Panyutin, and W.M. Bonner. 2002. Quantitative detection of (125)IdU-induced DNA double-strand breaks with gamma-H2AX antibody. *Radiat. Res.* 158:486–492. http://dx.doi.org/10.1667/0033-7587(2002)158[0486:QDOIID]2.0.CO;2

Sfeir, A., and L.S. Symington. 2015. Microhomology-mediated end joining: A back-up survival mechanism or dedicated pathway? *Trends Biochem. Sci.* 40:701–714. http://dx.doi.org/10.1016/j.tibs.2015.08.006

Singer, M.S., and D.E. Gottschling. 1994. TLC1: template RNA component of *Saccharomyces cerevisiae* telomerase. *Science.* 266:404–409. http://dx.doi.org/10.1126/science.7545955

Star, B., A.J. Nederbragt, M.H.S. Hansen, M. Skage, G.D. Gilfillan, I.R. Bradbury, C. Pampoulie, N.C. Stenseth, K.S. Jakobsen, and S. Jentoft. 2014. Palindromic sequence artifacts generated during next generation sequencing library preparation from historic and ancient DNA. *PLoS One.* 9:e89676. (published erratum appears in *PLoS One.* 2014. 9:e103170) http://dx.doi.org/10.1371/journal.pone.0089676

Sugawara, N., E.L. Ivanov, J. Fishman-Lobell, B.L. Ray, X. Wu, and J.E. Haber. 1995. DNA structure-dependent requirements for yeast RAD genes in gene conversion. *Nature.* 373:84–86. http://dx.doi.org/10.1038/373084a0

Takata, M., M.S. Sasaki, E. Sonoda, C. Morrison, M. Hashimoto, H. Utsumi, Y. Yamaguchi-Iwai, A. Shinohara, and S. Takeda. 1998. Homologous recombination and non-homologous end-joining pathways of DNA double-strand break repair have overlapping roles in the maintenance of chromosomal integrity in vertebrate cells. *EMBO J.* 17:5497–5508. http://dx.doi.org/10.1093/emboj/17.18.5497

Teixeira, M.T., K. Förstemann, S.M. Gasser, and J. Lingner. 2002. Intracellular trafficking of yeast telomerase components. *EMBO Rep.* 3:652–659. http://dx.doi.org/10.1093/embo-reports/kvf133

Torres-Rosell, J., I. Sunjevaric, G. De Piccoli, M. Sacher, N. Eckert-Boulet, R. Reid, S. Jentsch, R. Rothstein, L. Aragón, and M. Lisby. 2007. The Smc5-Smc6 complex and SUMO modification of Rad52 regulates recombinational repair at the ribosomal gene locus. *Nat. Cell Biol.* 9:923–931. http://dx.doi.org/10.1038/ncb1619

Wach, A., A. Brachat, R. Pöhlmann, and P. Philippsen. 1994. New heterologous modules for classical or PCR-based gene disruptions in *Saccharomyces cerevisiae*. *Yeast.* 10:1793–1808. http://dx.doi.org/10.1002/yea.320101310

Wong, J.M., L. Kusdra, and K. Collins. 2002. Subnuclear shuttling of human telomerase induced by transformation and DNA damage. *Nat. Cell Biol.* 4:731–736. http://dx.doi.org/10.1038/ncb846

Zampini, É., É. Lepage, S. Tremblay-Belzile, S. Truche, and N. Brisson. 2015. Organelle DNA rearrangement mapping reveals U-turn-like inversions as a major source of genomic instability in *Arabidopsis* and humans. *Genome Res.* 25:645–654. http://dx.doi.org/10.1101/gr.188573.114

Zhang, W., and D. Durocher. 2010. De novo telomere formation is suppressed by the Mec1-dependent inhibition of Cdc13 accumulation at DNA breaks. *Genes Dev.* 24:502–515. http://dx.doi.org/10.1101/gad.1869110

Zhao, X., and G. Blobel. 2005. A SUMO ligase is part of a nuclear multiprotein complex that affects DNA repair and chromosomal organization. *Proc. Natl. Acad. Sci. USA.* 102:4777–4782. (published erratum appears in *Proc. Natl. Acad. Sci. USA.* 2005. 102:9086) http://dx.doi.org/10.1073/pnas.0500537102

Zhao, X., E.G. Muller, and R. Rothstein. 1998. A suppressor of two essential checkpoint genes identifies a novel protein that negatively affects dNTP pools. *Mol. Cell.* 2:329–340. http://dx.doi.org/10.1016/S1097-2765(00)80277-4

Zhou, J., E.K. Monson, S.C. Teng, V.P. Schulz, and V.A. Zakian. 2000. Pif1p helicase, a catalytic inhibitor of telomerase in yeast. *Science.* 289:771–774. http://dx.doi.org/10.1126/science.289.5480.771

Zhu, Z., W.H. Chung, E.Y. Shim, S.E. Lee, and G. Ira. 2008. Sgs1 helicase and two nucleases Dna2 and Exo1 resect DNA double-strand break ends. *Cell.* 134:981–994. http://dx.doi.org/10.1016/j.cell.2008.08.037